Cell Mechanics Studied Using Atomic Force Microscopy

A Dissertation
presented to
the Faculty of the Graduate School
University of Missouri-Columbia

In Partial Fulfillment
of the Requirements for the Degree
of Doctor of Philosophy

---

by

Mingzhai Sun

Dr. Gabor Forgacs, Dissertation Supervisor

May 2008

The undersigned, appointed by the Dean of the Graduate School, have examined the dissertation entitled:

Cell Mechanics Studied Using Atomic Force Microscopy

presented by Mingzhai Sun
a candidate for the degree of Doctor of Philosophy
and hereby certify that in their opinion it is worthy of acceptance.

Dr. Gabor Forgacs

Dr. Shi-jie Chen

Dr. Christopher Hardin

Dr. Ioan Kosztin

Dr. Gerald Meininger

To my parents:

Aici Wang and Quanying Sun

and my wife:

Yanli Wang

ACKNOWLEDGMENTS

I want to express my deep admiration and profound gratitude to my supervisor Dr. Gabor Forgacs, who provided me the opportunity and all the conditions to explore an exciting research field. I am always amazed by his deep insight of the research. It is so enjoyable to have discussions with him. During the six years, he has been an excellent mentor, giving me the courage and guidance at the right time. He is also a good friend with whom I can share my joys and depressions. I appreciate the way and skills he guides us in the research. "Giving a man a fish, he will have a single meal, teaching him how to fish, he will eat all his life." Dr. Forgacs always tries to teach us how to fish. He offers me every possible opportunity to practice my presentation and writing skills, which are so important for a person who aims to stay in academia. An important reward for such effort was my predoctoral fellowship from the American Heart Association (AHA) in 2007.

I want to thank Dr. Michel Grandbois, who was my previous supervisor and later great collaborator. He recruited me from China and taught me the AFM technique. I also want to thank Dr. Wonchul Shin who picked me up in St. Louis airport after my 24 hours trip. Thanks to Dr. John Graham who provided me great help in learning the AFM technique.

Special thanks to my wonderful collaborator Dr. Irena Levitan from the University of Illinois at Chicago. I appreciate her help and invaluable input to my AHA proposal and the cholesterol research project.

I feel so fortunate to be surrounded by the nice people in our group. I would like to show my appreciation to the former and present members, with whom I had the pleasure to work with: Dr. Francoise Marga, Dr. Adrian Neagu, Dr. Karoly Jakab, Dr. Basarab Hosu, Dr. Brooke Damon, Dr. Zhongkui Hong, Marius Sticulescu and Cyrille Norotte.

Thanks to my wife, Yanli Wang, who helped me in a hundred ways. It would have been impossible for me to concentrate on my research without her taking care of the whole family. I am also thankful to her parents who help me looking after my lovely son Weihong Sun.

I own a great debt to my parents Aici Wang and Quanying Sun, for their help, love and support. I hope I make them proud.

Contents

List of Tables

List of Figures

Chapter 1

Introduction and Background

In this chapter, I will first present the organization of the dissertation and then briefly review the development of the Atomic Force Microscopy (AFM) and its applications in the life sciences.

1.1 The organization of the thesis

The first chapter provides a simple review of the AFM, which is the main tool used in this study. The second chapter collects all the employed methods and techniques. Chapter three is a systematic study of membrane tethers with the AFM technique. Chapter four focuses on the cholesterol effects on endothelial cell mechanics using the methodology developed in chapter three. In the last chapter, the two classes of theories on tether formation are compared with the experiments.

1.2 The AFM

In 1986, Binnig et al. [6] invented the AFM based on the Scanning Tunneling Microscope (STM). Compared with STM, AFM has much less restrictions on sample preparation, which greatly extends its applicability. For example, STM can only be used on conductive samples, while normally there is no need for surface modification on the AFM samples.

The AFM consists of three major components (Fig. 1.1): a force transducer, an optical detection system [1, 34] and the piezoelectric elements. The force transducer is a cantilever (Fig. 1.1), which acts as a soft spring. The delicate movement of the cantilever is recorded by the optical detection system, which includes a laser generator, and a two- or four-sector photodiode. In essence the laser beam is focused on the cantilever and the reflected beam is recorded by the photodiode. Changes in the voltage on different sectors of the photodiode are used to determine the force exerted on the cantilever. To keep the force constant, there is a feedback loop, which controls the piezoelectric element to modulate either the sample or the cantilever position.

As the force transducer, the cantilever plays a critical role in the AFM measurement. It determines not only the measurable force range but also the noise to signal ratio. On one hand, one wants to maximize the deflection of the cantilever to detect very small forces. This requires the cantilever to be as soft as possible. On the other hand, according to the energy partition theorem, the vibrational amplitude (x) of the cantilever can be estimated by $x = \sqrt{\frac{k_B T}{k}}$, where k_B is the Boltzmann constant, and T is the absolute temperature. It is obvious that

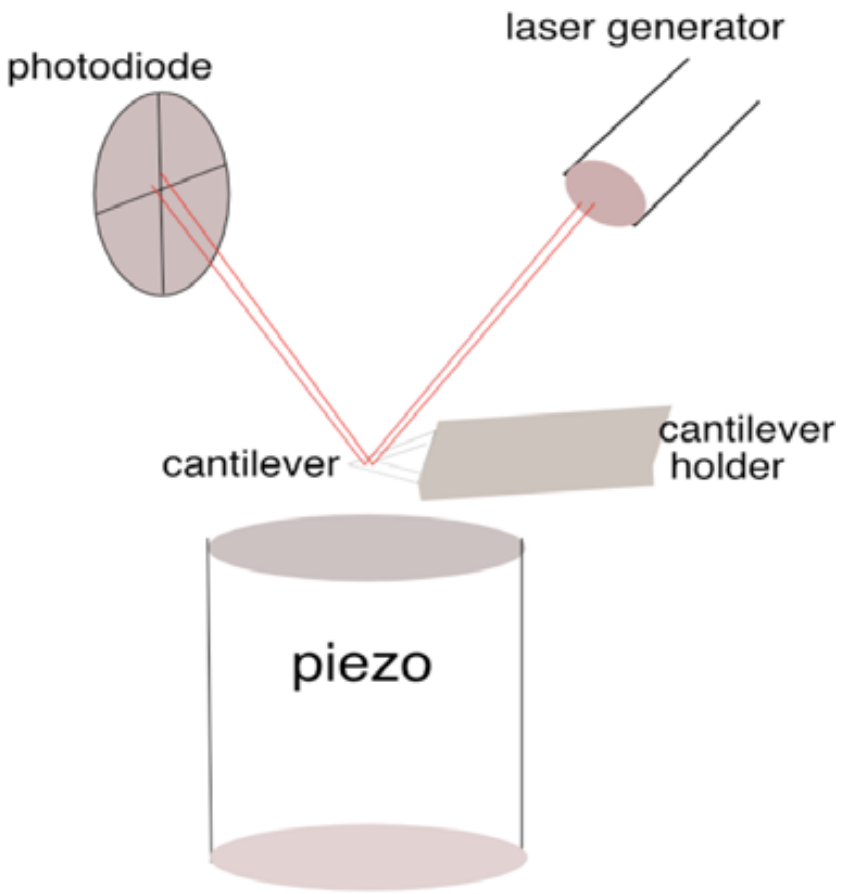

Figure 1.1: Schematics of the AFM. The photodiode and laser generator form the optical detection system; the piezo controls the movement of the sample and the cantilever is the force transducer.

the smaller the spring constant (k), the bigger the thermal vibrational amplitude (x). In addition, to reduce the sensitivity of the cantilever to the external vibration, the resonance frequency of the cantilever should be far from the frequency of the external vibration source, such as the vibration of the building, which is around 100 Hz. The cantilever's resonance frequency (f_0) can be estimated by $f_0 = \frac{1}{2\pi}\sqrt{\frac{k}{m_0}}$ where m_0 is the mass of the cantilever. This obviously puts another limit on the spring constant of the cantilever. Cantilevers used in this study have

spring constant 0.01 N/m , and the softest cantilever currently available has the spring constant 0.006 N/m.

To get accurate force measurement, the spring constant of a cantilever should be calibrated before experiments. There are multiple methods for cantilever calibration, such as reference spring [99], added mass [84] and thermal fluctuation [47]. Due to its simplicity, thermal fluctuation method has been very widely used. Two steps are needed in this method. First, the cantilever touches a hard surface (usually a cover glass or a mica) to get the voltage-extention curve, and then a linear fit is done to get the slope (V/m) (Fig. 1.2 A). Second, a power spectrum of the cantilever is recorded in the experimental environment (buffer or cell culture medium) and the area of the power spectrum is calculated (Fig. 1.2 B). The spring constant of the corresponding cantilever is given by [47, 71, 84]

$$k = 0.8 k_B T \frac{slope^2}{Area}$$

where k_B and T are the Boltzmann constant and temperature respectively. This procedure is usually complicated by measurement noise. High pass filter was integrated in the hardware to filter out the low frequency noise (especially the 60 Hz electronic noise). Software filter is also frequently used to post-process the collected data [39]. In all the presented experiments, thermal fluctuation method was used to calibrate the cantilevers. It yielded spring constant values in the range [7, 13] pN/nm, in agreement with the manufacture value of 10 pN/nm.

In recent years, AFM has gained great popularity in the biological sciences.

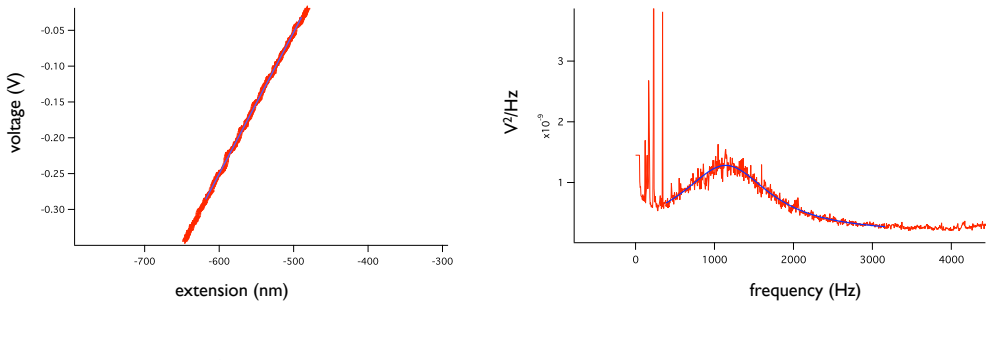

the graphicx package

Figure 1.2: Calibration of AFM cantilevers. A. Linear fit to the voltage-extension curve to obtain the slope. B. Lorentzian fit to the power spectrum. The area under the spectrum is calculated.

Compared with conventional imaging methods, AFM provides not only sample morphology, but also can mechanically stress the samples and generate quantitative response. For example, AFM provides biologists a great opportunity to investigate the response of cells to external mechanical stimulations.

To get topographical information on a sample, one can use two AFM operating modes: contact mode and tapping mode [53]. In the contact mode, the cantilever is brought into continuous contact with the sample. To avoid moving the sample, the sample may be trapped in pores of filters, or strongly attached to the substrate. In the tapping mode, the cantilever intermittently contacts the sample, which reduces the frictional force and contact time and allows to minimize the deformation of the biological sample. This mode is suitable to image fragile or loosely attached samples. Many cell types were imaged using AFM by either contact mode or tapping mode.

Besides the morphology, AFM measurement also provides information on the mechanical properties of the sample. Fig. 1.3 shows how to use AFM to measure cell mechanical properties. At first (Fig. 1.3 A) the cantilever is far away from the cell, then it approaches the cell either by moving up the sample holder or by lowering the cantilever to form a contact (Fig. 1.3 B, C). Next, the cantilever is separated from the cell (Fig. 1.3 D). During this process, the deflection of the cantilever and the movement of the piezo are recorded to form the force-extension curve as shown in Fig. 1.3 (see the plot in the middle). By analyzing the indentation curve based on the Hertz or Sneddon model [72, 94], the elastic modulus of the cell can be extracted.

As another noticeable application, recently AFM has been used to measure cell-substrate or cell-cell interactions. For cell-substrate adhesion, usually a cell is attached directly to the cantilever (or through a bead which attaches to the cantilever) and then approached to a chemically treated substrate. If the substrate is covered by other cells or even a cell layer, then cell-cell interactions can be measured. This approach can measure adhesion at the molecular level [109].

When it was invented, AFM was mainly used in the material sciences and was difficult to measure samples in the liquid environment, which is usually required for the biological samples. Now, with the modern AFMs, samples can be in medium with the ambient temperature well controlled. This is critical for experiments needed to be done under physiological conditions. Another development of AFM is to combine AFM technique with other optics (e.g. total internal reflection fluorescence microscope (TIRF), fluorescent resonance energy transfer (FRET)). By combining the AFM with fluorescence microscopy, one can mea-

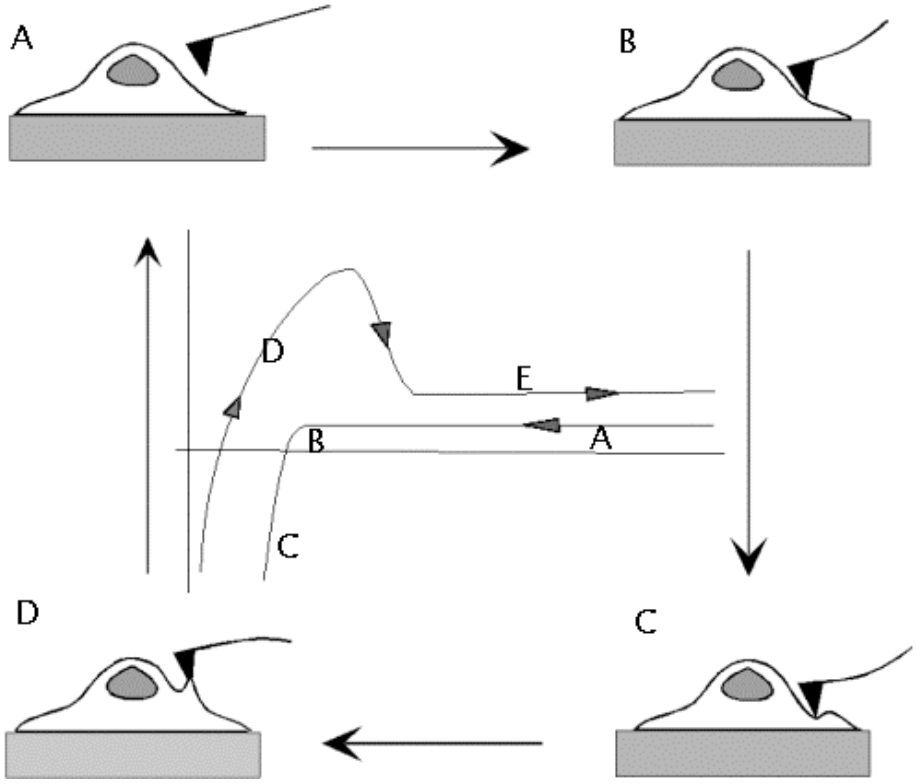

the graphicx package

Figure 1.3: Force-extension curve. (A) The cantilever is far from the cell and there is no interaction between it and the cell. (B). The cantilever approaches the cell either by lowering it or moving up the sample holder to form contact. (C). Further approach leads to bigger cantilever and cell deformation. (D). The cantilever starts to separate from the cell. The attraction force (specific and non-specific) deforms the cantilever in the opposite direction. (E). The cantilever gets back to the original location as in (A). The cantilever is far from the cell. The middle panel shows the force-extension curve corresponding to the described cycle. The gap between part A and E, part A and the x-axis are shown only for clarity. In reality they coincide (both sections correspond to the movement of the free cantilever). (Modification based on the figure in [53]).

sure cell mechanics while simultaneously monitoring the fluorescence to check cell response. This provides a unique way to investigate cell mechanical signaling pathways. For example, reference [100] shows that applying a force to the apical surface of vascular smooth muscle cells induces cytoskeletal response and results in the change of the focal contact reorganization in the basal sides of the cells [100]. In the present study, we combine the AFM with an epifluorescence microscope. This enables us to select cells that are genetically transfected to express the green fluorescence protein (GFP).

The Home-built Force Spectroscope

The instrument used in the study is a home-built, AFM based force spectroscope. It is specifically designed for force measurement. It resides on the stage of an inverted microscope, housed in a customer-built chamber that allows modulating and controlling the temperature (Fig. 1.4 A, B). The piezo's traveling range is about 30 μm, which is needed for the measurement of cell membrane tethers (explained in the next chapter) with the micrometer length scale.

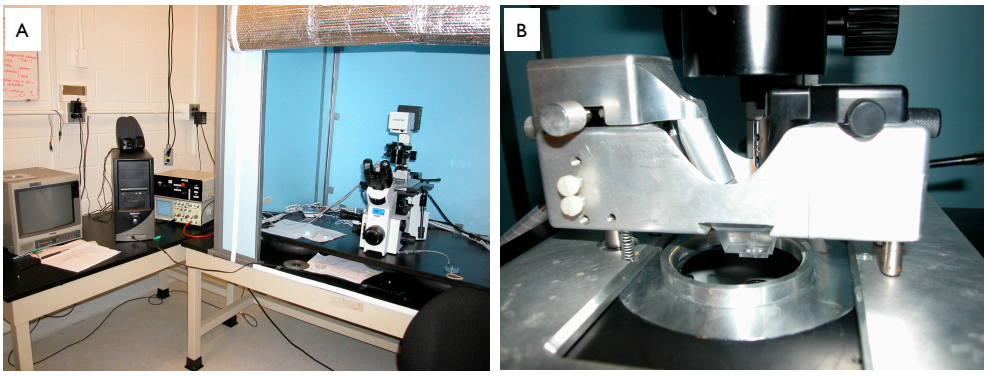

Figure 1.4: The home-built AFM. A: AFM with controller, monitor and the inverted microscope. B: Magnified view of the AFM on the stage of an inverted microscope.

The force spectroscope is controlled with the custom-written software using Igor Pro and the NIDAQ Tools MX package. It contains three main modules: power spectrum acquisition, hard surface calibration, measurement control and the analysis module (Fig. 1.5).

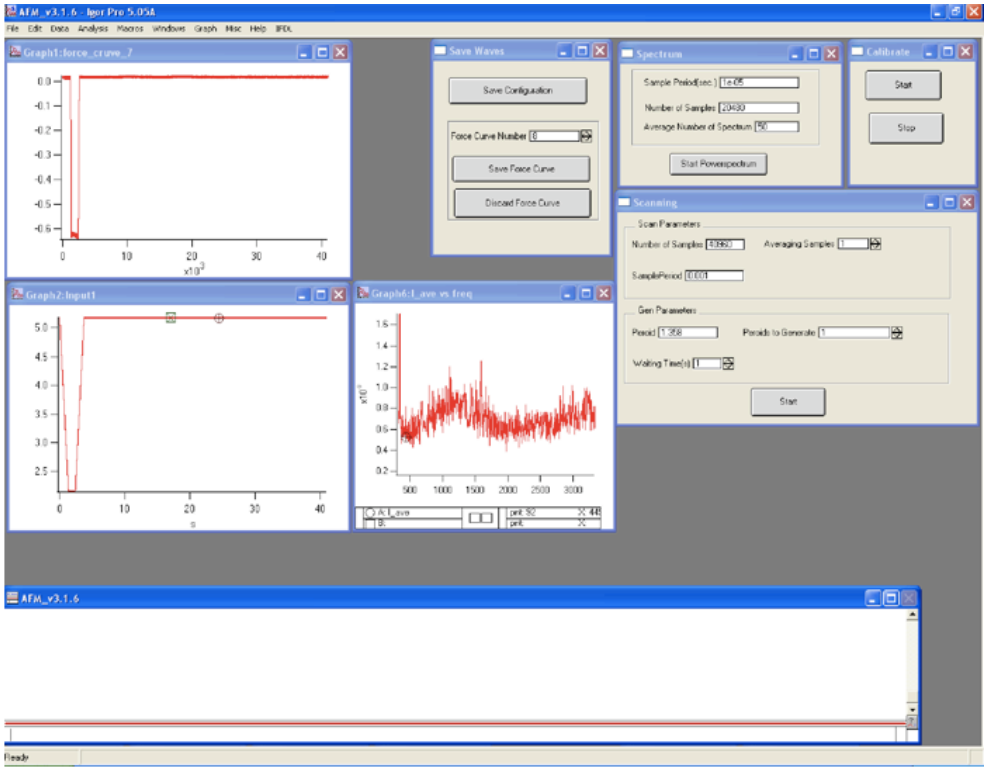

Figure 1.5: The graphic user interface of the force spectroscope control software.

Chapter 2

Employed Methods and Techniques

2.1 Cell culture and treatment

Common cell culture condition

Cells are cultured in DMEM (Invitrogen, Carlsbad, CA) containing 10% fetal bovine serum (FBS, Sigma-Aldrich, St. Louis), 10 μg/ml penicillin, streptomycin and kanamycin sulphate (Invitrogen Corp., Carlsbad, CA). Cells were maintained in a humidified incubator at 37^oC with 5% CO_2.

Specific conditions for different cell lines

Bovine aortic endothelial cells (BAECs; Cambrex East Rutherford, NJ) between passages 12 and 20 were used in the study. Cells were split every 3-4 days. The

human brain tumor cell line (HB) [41] was cultured with 5 μg/ml fungizone. The human endothelial cells EA hy926 were a generous gift of Dr. C-J S. Edgell [27], and were maintained in HAM'S F-12 supplemented with 20% fetal bovine serum (Sigma-Aldrich).

Latrunculin A and hyaluronidase treatment

In cytoskeletal disruption experiments, the cells were in regular medium supplemented with latrunculin A (Sigma), a specific actin polymerization inhibitor [18, 106] at various concentrations (0.1, 0.2, 0.5, and 1.0 M) for 30 min before the measurement. The importance of the glycocalyx in the fomation of membrane nanotubes was studied through one of its major components, the glycosaminoglycan hyaluronan [107]. The removal of hyaluronan from the surface of substrate-attached cells was achieved by a 30-min incubation in the presence of hyaluronidase (500 IU/ml) (Sigma-Aldrich) in serum- and polysaccharide-free medium.

Cellular cholesterol modulation

BAECs were enriched with or depleted of cholesterol by incubating them with methyl-β-cyclodextrin (MβCD) saturated in cholesterol or using empty MβCD (not complexed with cholesterol), as described in previous studies [57]. Free cholesterol mass analysis was done by gas-liquid chromatography (GLC) (as described in e.g., Levitan et al., [57]). Cell protein content was determined on the lipid-extracted monolayer using a modification of the method of Lowry et al. [61].

All mass values were normalized on the basis of cell protein.

2.2 Force spectroscopy measurements

Sample preparation

Typically, around $5x10^4$ cells were plated on bare or different substance coated glass coverslips (Pierce Biotechnology, Rockford, IL), placed in 35-mm plastic petri dishes (Techno Plastic Products, Trasadingen, Switzerland), and cultured at 37^oC in a 5% CO_2 incubator for 24 h before AFM measurement.

Cantilever and substrate modification

For surface modification assays, cantilevers (Veeco, Santa Barbara, CA) and glass coverslips (Pierce Biotechnology) were put in 0.1 mg/ml Poly-L-Lysine solution (Sigma) for 15 min, then rinsed with Milli-Q water (Millipore, Billerica, MA) and air-dried. The effect of a collagen-coated surface was evaluated by incubation of cantilevers in a type I collagen solution (1 mg/ml; Sigma) at 4^oC for 60 min, and subsequent rinsing with Milli-Q water and air-drying in a laminar flow hood.

Tether force measurement

Our in-house-built force measurement device, based on the design and operation of an AFM, was attached to the stage of an inverted optical microscope (Olympus IX70, Olympus America, Melville, NY). This arrangement allowed for precise positioning of the cantilever on the area of interest along the cell membrane.

Soft silicon nitride cantilevers (Veeco, Santa Barbara, CA) were cleaned in 70% ethanol, rinsed in Milli-Q water, and then sterilized with UV light for 15 min. Each cantilever was calibrated before a given experiment using thermal noise amplitude analysis [10, 11, 47]. The measured spring constants were between 7 and 13 mN/m, in agreement with the nominal spring constant of 10 mN/m.

A 60-mm Petri dish containing cells in CO_2 independent medium at room temperature, supplemented with 10 μg/ml penicillin, streptomycin, and kanamycin sulphate, was placed under the AFM. A typical experiment was performed as follows: the cantilever was moved toward the surface until contact with the cell membrane (observed from the deflection of the cantilever) was established. Contact was maintained for 2 – 30 s, and then the cantilever was retracted from the cell surface. Loading rates were varied according to different experiments (a range from 1 μm/s to 40 μm/s). Force elongation profiles were recorded using a number of cells from each cell type, with each cell subjected to multiple retraction experiments. Several hundred discrete events were used for data analysis. Data analysis was carried out with Igor 4.09 (WaveMetrics, Inc. Lake Oswego, OR).

2.3 Visualization of membrane nanotubes with quantum dot-labeled cells

Endothelial cells (EA hy926) were washed three times in phosphate-buffered saline (Fisher Scientific, Pittsburgh, PA) to remove culture medium followed by

incubation with sulfo-NHS-biotin (Sigma, St. Louis, MO) at a concentration of 100 μg/ml for 15 min at room temperature. Subsequently, cells were washed four times in HAM'S F-12 cell culture medium (Wisent, St. Bruno, Canada) and incubated with streptavidin-conjugated Q-dots (Quantum Dot, Hayward, CA) with a fluorescence maximum at 605 nm. Finally, cells were rinsed an additional three times to remove unbound Q-dots and micrographs were obtained with an inverted epifluorescence microscope (Axiovert 200, Zeiss, Thornwood, NY) on which the force spectrometer was mounted. Images were taken (40x objective) with an ME2 CCD camera (Finger Lakes Instrumentation, Lima, NY) at a resolution of 768 x 512 pixels. Membrane tethers were formed by contacting an individual cell with the AFM cantilever, followed by a simultaneous vertical and lateral retraction allowing individual tether visualization.

2.4 Confocal Fluorescence Recovery After Photobleaching (FRAP)

For $DiIC_{12}$ labeling cells were incubated with 0.5 μg/ml of $DiIC_{12}$ (stock 5 mg/ml in DMSO) in DMEM without FBS for 20 minutes. Confocal FRAP was performed as described by Kenworthy et al. [50]. Briefly, a Zeiss LSM 510 Meta NLO 2-photon confocal (Carl Zeiss, Thornwood, NY) was used with a 63x 1.4 NA Zeiss Plan Apochromat oil immersion objective, at a digital zoom of 2, a scan speed of 10, and the pin-hole set at 1 Airy units. Prebleach and postbleach images were acquired using low laser intensity. Photobleaching was performed

using 10 scans with the 800 nm laser line at 10 % transmission in a rectangular region of interest, 4 μm wide. All FRAP measurements were carried out in CO_2 independent medium at room temperature. In case of cytoskeleton disruption experiments, prior to measurement, cells were treated for 10 minutes with latrunculin A, as described above.The effective diffusion coefficients were determined from the postbleached image series using a program that compares the experimental and simulated recoveries into the bleached region [93].

2.5 Visualization of the actin cytoskeleton and cell morphology

To visualize the microfilament network, F-actin staining was performed using standard procedure. Cells were fixed in 4% paraformaldehyde (PFA) for 10 min, permeabilized with 0.1% Triton-X100 for 5 min, incubated with PBS (2% FBS) for 15 min, and subsequently with 0.1 μM Rhodamine-Phalloidin (Sigma, St. Louis, MO) for 20 min. After each step, samples were rinsed three times in PBS. Images were acquired using a BioRad Radiance 2000 (Carl Zeiss Microimaging Inc. Thornwood, NY) confocal system. Cell morphology as function of cholesterol treatment was visualized with Differential Interference Contrast (DIC) microscopy. Images were acquired using the DIC imaging module on the Zeiss LSM 510 Meta NLO 2-photon confocal (Carl Zeiss, Thornwood, NY) with a 63x 1.4 NA Zeiss Plan Apochromat oil immersion objective. In order to minimize the bias, blind experiments were performed. Control and cholesterol treated cells

were cultured on the same cover glass (appropriately partitioned in two regions) by one individual and subsequently imaged by another individual without the knowledge of which region contained the treated and control cells.

2.6 Determination of membrane surface viscosity

There are different theories for the analysis of the tether force (F_0) as a function of tether growth velocity (V_t; in our case the AFM cantilever retraction speed) including power law [8, 29, 42] and linear relationships [44]. In our experimental regime, the linear relationship worked well. In this case, as analyzed by Hochmuth et al. [44], $F = F_0 + 2\pi\eta_{eff}V_t$. Here η_{eff} is the effective surface viscosity and F_0 is the threshold force for extracting a tether. F_0 is given by $F_0 = 2\pi\sqrt{2TB}$, where the apparent membrane tension T provides a direct measure of the membrane-cytoskeleton adhesion and B is the membrane bending stiffness [92].

2.7 Bond force computation

Leukocytes circulating in the blood flow occasionally collide with the endothelial wall, which may result in tether formation, from either the endothelial or leukocyte membrane. The force, due to shear stresses in the blood flow, acting on the adhesive bond between the tip of the tether and the apposing membrane (i.e. selectin-PSGL-1 ligand), F_b, can considerably be reduced by the extension of the

tether [89]. We investigated how cholesterol, through its effect on the mechanical properties of endothelial tethers may influence F_b. Using the parameters (F_0 and η_{eff}) from the tether pulling experiments, F_b can be calculated from the following equation

$$F_b(L) = F_0 + 2\pi\eta_{eff}\frac{dL}{dt} \tag{2.1}$$

where $L(t)$ is the instantaneous tether length. We solved Eq. 2.1 numerically for endothelial tethers, formed under various cholesterol conditions, using the model of Shao et al. (Shao, 1998). These authors established the conditions of force and torque balance for a neutrophil (along with an equation expressing the geometry of the neutrophils attachment to the endothelium, assuming attachment through a single tether). In the computation, the radius of the leukocyte and shear stress due to blood flow were assumed to be 4.25 μm and 0.08 pN/ m2 respectively.

2.8 Statistical analysis

Analysis of covariance was used to compare the results of tether pulling experiments under different conditions. For the FRAP data comparison, Students t-test was used [108].

Chapter 3

Membrane tethers extracted by AFM

AFM has been used in the biological sciences for many years. One of its applications is to measure cell mechanical properties. The conventional method for such purpose is to use the cantilever to indent the cell surface and study, for example, the Young's modulus of the cell. In this chapter, an alternative method – membrane tether pulling – is presented to investigate cell mechanics.

3.1 Cell membrane structure

Cell membrane is one of the most important structures of a cell. It encloses a cell and defines its boundary. The two most dominant components of the cell membrane are the phospholipids and the membrane proteins. The phospholipids form the membrane bilayer (Fig. 3.1), which provides the basic fluid structure of

the membrane. The membrane proteins perform most of the functions, such as selective permeability. Outside of the lipid bilayer is a macromolecular network called glycocalyx (Fig. 3.1). It is mainly composed of polysacchrides (one of most important components being hyaluronan). The glycocalyx protects the cell from mechanical damage and other harmful chemical exposure. Recent experiments also indicate that it may be involve in signal transduction, cell adhesion and cell motility [52, 55]. Underneath the bilayer is the cytoskeleton structure of a cell (Fig. 3.1), which plays important role in cell shape, cell migration and cell-cell communication. The cytoskeleton is made of three major components, actin filaments, intermediate filaments and microtubules. In normal cells, the cell membrane strongly connects to the cytoskeleton through transmembrane proteins and some lipid molecules such as PIP2 [77].

3.2 Membrane tethers

Tethers are nanotubular structures emanating from the cell membrane. They can be formed in vivo and in vitro by variety of force transducers, such as AFM cantilever [98], micro-beads [23, 46, 88], and even cells [5]. These cylindrical nanotubular structures are mainly made of phospholipids. So far, there is no experimental evidence showing cytoskeleton structures (especially F-actin) inside these structure [77], at least for tethers extracted in vitro. Due to its small size (only about 50 nm in diameters), nanotubes can hardly be seen with the optical microscope. Using differential interference contrast microscope (DIC) [24] and fluorescence microscope with either membrane dyes [59] or quantum dots [98],

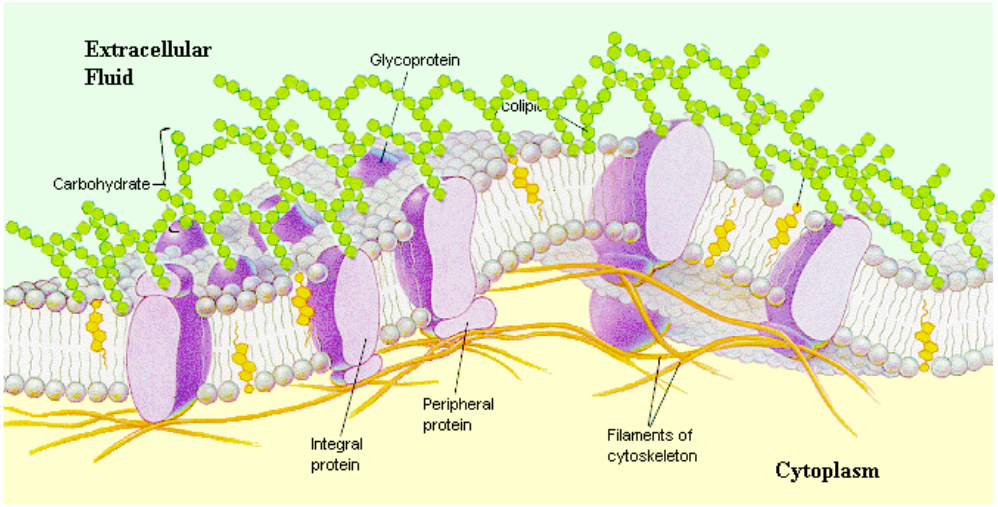

Figure 3.1: Membrane structure. Cell membrane is mainly made up of phospholipids and membrane proteins. The phospholipids form the membrane bilayer. Outside of the lipid bilayer, there is a "cell coat" called glycocalyx. It is mainly composed of polysaccharide chains. Underneath of the bilayer is the cytoskeleton. Modification based on http://sun.menloschool.org/~birchler/cells/plants/cell_membrane/cellmembrane.jpg.

tethers have been visualized. However, in all these cases, what have been seen are most likely bundles of membrane tethers instead of a single tether. Recently, Hosu and coworkers [46] used magnetic tweezers to extract membrane tethers, then fixed the system with fixatives to visualize tethers with a scanning electron microscope. This way individual tethers could be visualized. These acquired SEM images also suggest that, at least in case of the magnetic tweezers, tethers may be pulled from the pre-existing structures, more specifically microvillies. These tethers are relatively homogeneous with diameters of 50 nm (Fig. 3.2).

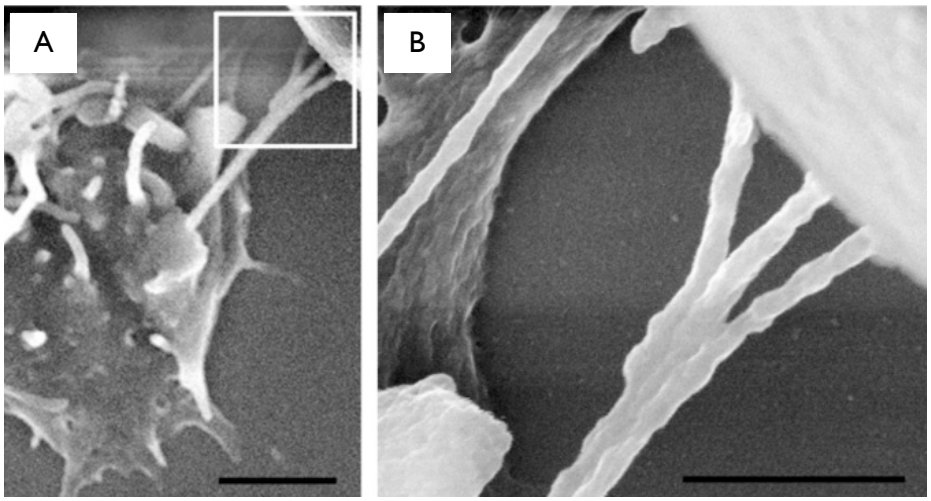

Figure 3.2: Scanning electron microscope image of membrane tethers from HB cells [46]. A: lower magnification. B: high magnification. Scale bars: 1μm in A; 500 nm in B.

Tethers exist in vivo and play important roles

Membrane tethers form in vivo and fulfill multiple biological roles. First, in combination with adhesion molecules such as P or E-seletins, they form an "automatic braking system" [14] for cells in the blood flow to slow down and get

arrested (i.e. attach to the blood vessel wall). Second, membrane tethers provide inter- and intra- cellular signaling pathway.

During an inflammatory process, leukocytes (e.g. monocytes, neutrophils) in the blood flow need to slow down from the blood flow, adhere to the endothelium and finally transmigrate through the endothelium. The initial steps (i.e slowing down and attachment to the endothelium) involve a variety of adhesion molecules, such as selectins and immunoglobulin superfamily cell adhesion molecules (CAMs). The dynamics of these adhesion molecules have been extensively investigated. However, the involvement and importance of the membrane tethers were recognized and experimentally proved much later. In 2002, Eric Park and coworkers [68] performed a series of experiments showing the important role of the membrane tethers in the neutrophil rolling process. They used a cell-scaled microbead system to monitor motion of the neutrophils and PSGL-1 coated beads of similar size in a parallel plate flow chamber with P-selectin coating. The motion patterns of the beads and neutrophils turned out to be very different. Beads manifested unstable, intermittent movement, with velocities well predicted by hydrodynamic considerations. The pauses between successive velocity spikes were very short. Under the same condition, neutrophils showed more even motion with considerably smaller velocities and longer pauses between velocity spikes than found in case of the beads. However, after the neutrophils are fixed with glutaraldehyde (thus not able to sprout tethers), their motion resembled that of the beads. This experiment demonstrated that membrane tethers can stabilize neutrophils rolling, which was confirmed by further experiments using a cell-cell assay [73, 87]. Tether formation is not the unique mechanism in

the inflammatory response. It is also relevant in cancer metastasis [64].

Another important biological function of membrane tethers is that they provide a pathway for intracellular and intercelllar communication [49, 83, 101]. It was first shown by Rustom and coworkers [83] that membrane tethers can connect cells and provide intercellular highways for signaling and mass transport. A very recent article by Sowinski and coworkers demonstrated that HIV-1 may transfer over long distances with high efficiency, utilizing membrane tethers connecting T cells [95]. Inside cells, tethers can also form among organelles and participate in signaling and mass transport [101].

3.3 Tether extraction by AFM

Several experimental methods have been used to characterize the mechanical properties of membrane tethers, such as optical tweezers [23, 25, 58] and micropipette aspiration assays [32, 33, 44, 45, 48, 103]. In the optical tweezers experiments, a micro-bead is held by the laser and a cell is approached to the bead to form contact, then either the cell or the bead is moved away so that tethers can be extracted. The force on the bead can be read out and a force vs. time curve is plotted. A well defined plateau is observed in the curve. This can be understood in terms of a membrane reservoir being gradually depleted upon pulling on the bilayer [74]. In the micropipette experiments, a cell is held with a pipette while a spherical bead is held with another. At the beginning, a well controlled positive pressure is applied to push the bead to contact the cell held by the other micropipette. Then, a negative aspiration pressure is imposed to pull the bead

away. The displacement of the bead vs. time is recorded and plotted. From the displacement vs. time curve, the speed of the bead is calculated. Information on tethers can be drawn by comparing the speeds of the bead with and without tethers.

The AFM provides another way to investigate membrane tethers. In the AFM experiments, the cantilever approaches a cell to form a contact, remains on the cell surface for a controlled time period and then retracts from the cell. The force on the cantilever can be monitored by the photo-detector (Fig. 3.3).

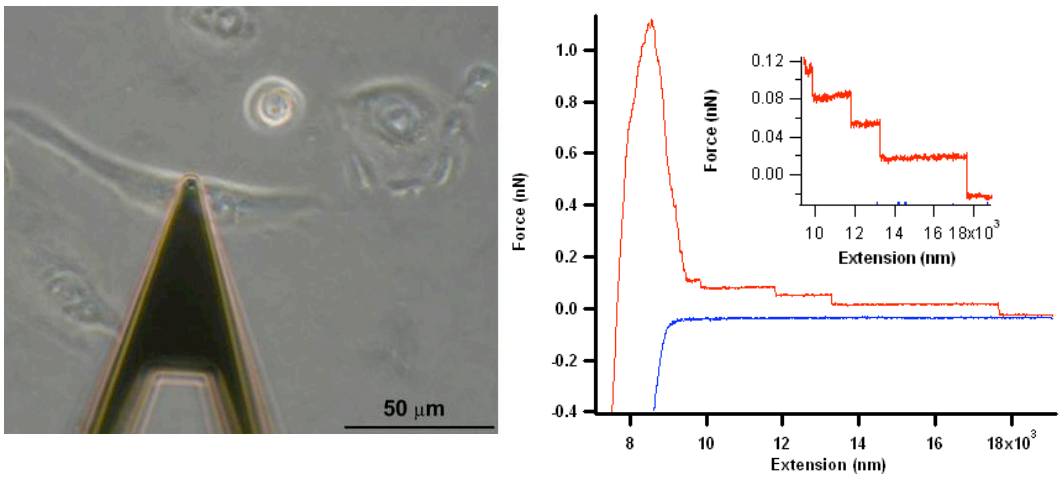

Figure 3.3: A: The optical image showing positioning of the cantilever on the cell surface. B: A typical experimental force curve. The blue curve corresponds to the approaching of the cantilver to the cell surface; the red one corresponds to the retraction of the cantilever from the cell surface. On the retraction curve, multiple step-like structures are clearly resolvable. The inset is the magnified version of the step-like structures.

Compared with the micropipette technique, the AFM method has several advantages. First, the speed to approach or retract from the cell can be controlled much more accurately with a piezo. Second, tether forces as low as 10 pN can be

achieved with considerably higher accuracy than with micropipettes. Though the force resolution can be sub-peco newton with an optical tweezers, the maximum force it can apply is very limited (usually lower than 100 pN). This limitation of the optical tweezers makes it hard to simultaneously extract multiple tethers. As shown in Fig. 3.3 B, with the AFM, forces in excess of 1 nN can be achieved, far beyond the capability of the optical tweezers.

3.3.1 Multiple tether formation and rupture

Tether formation during cell movement and cellular adhesion is likely to involve the simultaneous formation of multiple tethers. The tether pulling experiments performed until now have primarily addressed the formation of single tethers. One recent study explored dual tether extraction using the micropipette aspiration technique. Here the tethers were observed not in force-elongation profiles, but rather through the analysis of the dependence of the pulling force on the growth velocities of the tethers [104]. Other recent work has demonstrated that multiple membrane tethers can be formed in a minimal system composed of a giant unilamellar vesicle, kinesin-coated beads, microtubules, and ATP as energy source [51, 56, 82]. Beyond these examples, little is known about the behavior of multiple, simultaneously existing tethers in real cells, and their coupling with the overall membrane reservoir or their association with each other. Whether or not multiple membrane tethers can be simultaneously extracted from the membranes of living cells is still a matter of controversy.

In a recent theoretical article, Derenyi et al. [26] predicted that, in the ab-

sence of pinning forces, multiple membrane tethers coalesce smoothly. This study also points out that in real cells, membrane heterogeneities or coupling to the cytoskeleton may prevent tether fusion. However, there is no experimental evidence for the prediction.

To extract multiple tethers, a large initial adhesion force has to be overcome (Fig. 3.3 B). A force transducer with the ability to measure a broad range of forces (such as those encountered in specific and nonspecific cellular adhesion events) is needed. The AFM has the ability to apply a large range of forces (picoNewtons to nanoNewtons) (Fig. 3.3 B). This provides the opportunity to simultaneously monitor the formation of individual or multiple tethers and to bring new insight into the behavior of multipally extracted tethers. In this study, we used the AFM to extract multiple tethers, using a variety of cells with different morphology and origin, including Chinese hamster ovary (CHO) cells, a malignant human brain tumor cell line (HB), and endothelial cells.

In a typical AFM pulling experiment, the cantilever approaches the cell surface and is in contact with it for about 10 seconds before it retracts. Fig. 3.3 B shows a typical force-extension curve, with the blue approaching curve and red retraction curve. On the retraction curve, there are multiple step-like structures, which we identify with the detachment of individual tethers from the cantilever for reasons that will be further discussed in the following.

3.3.2 Visualization of membrane tethers with quantum dots

Formation of membrane tethers between cells and untreated AFM cantilevers was demonstrated by labeling the cell surface with fluorescent quantum dots and probing the cell in a manner similar to that used in the force measurements. Fig. 3.4 shows a membrane tether/tethers formed after contact of the AFM cantilever with an endothelial cell. The two fluorescent images correspond to two different positions of the cantilever and demonstrate the fluid nature of membrane tethers.

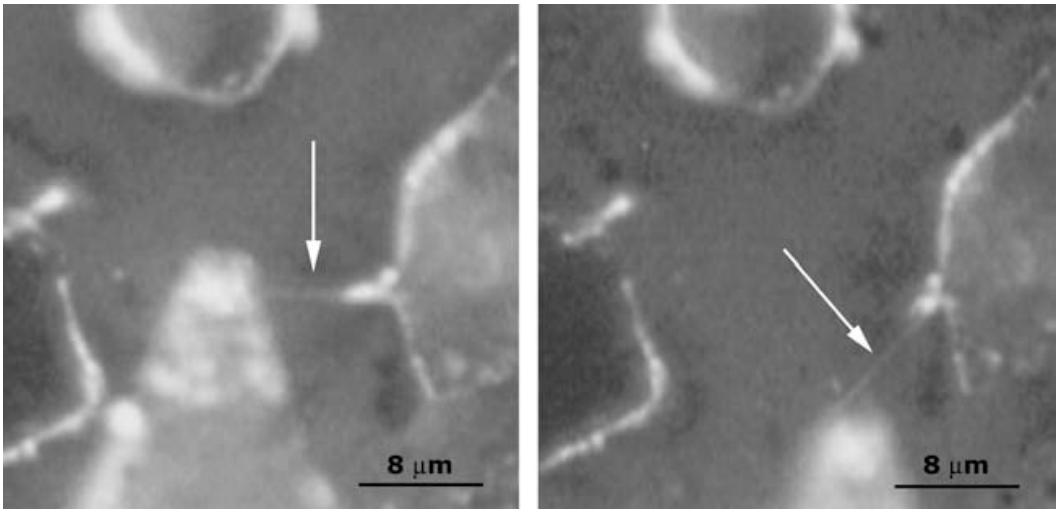

Figure 3.4: Tethers pulled by horizontal movement of the cantilever are observed by labeling the cell membrane with fluorescent quantum dots. The arrows indicate the tethers, which move freely as they follow the movement of the cantilever [98].

This visual control provides confirmation that the features present in the retraction profiles (Fig. 3.3 B) are the result of tether extraction from the cell

membrane. However, fluorescence imaging did not permit resolving multiple tethers, possibly due to their close proximity to each other and small diameter.

3.3.3 The tether force

The retraction profiles recorded with three different cell types exhibited an initial high force region followed by distinct, multiple plateaus separated by force steps (Fig. 3.5). The existence of the high force region indicates that, to initiate the tether extraction process, a substantial effort is needed. The height of this region, as well as the number of plateaus in a given retraction experiment, were found to be sensitive to the duration of the initial contact between the cantilever and the membrane, but the magnitude of the force steps between plateaus, ΔF, was not.

In previous experiments, performed with optical traps, plateaus in force-elongation profiles were associated with the pulling of individual membrane tethers ("tether force" in what follows), composed of freely diffusing membrane components, mainly phospholipids and membrane proteins [74]. The length of the plateau was correlated with the extent of the membrane reservoir.

In most of our experiments, multiple plateaus were observed along the entire extension, and within an individual force-extension profile. Since the discrete force steps between consecutive plateaus were markedly comparable (Fig. 3.5), we interpret them as the simultaneous elongation and sequential loss of multiple membrane tethers formed between the cell and the cantilever. Consequently, ΔF, the change in force between two consecutive plateaus, can be associated

with the force needed to pull a single tether, which we define as the membrane tether force F (with values shown in Table 3.1 for various cell types and treatment conditions).

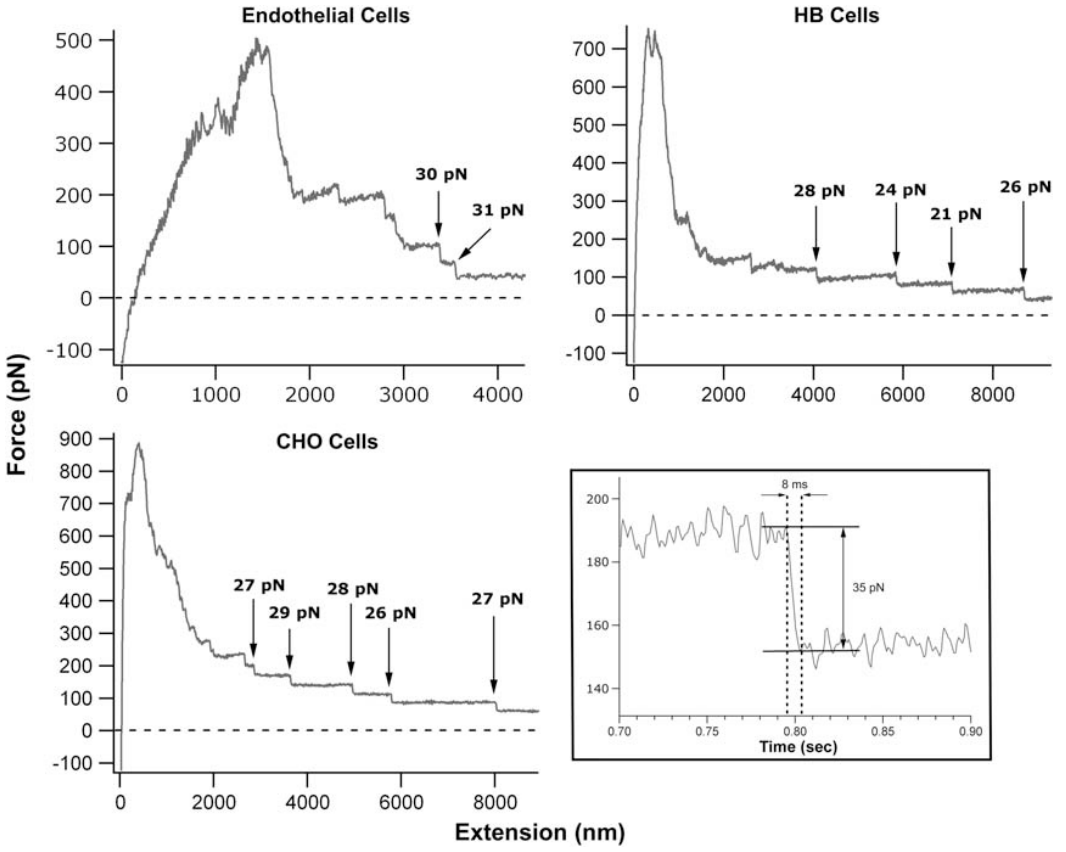

Figure 3.5: Typical retraction-force curves as function of cantilever extension for three cell lines. Numbers on the graphs denote the values of the individual force steps between consecutive plateaus. Note the very similar force drops in the quasi-constant force elongation regime. The fact that zero force is not reached at the end of the retractions, indicates that tethers are still attached. Inset shows timescale for a typical force drop [98].

		Latrunculin A treatment				Hyaluronidase
	Control	0.1 μM	0.2 μM	0.5 μM	1 μM	500 IU/ml
Endothelial cells	29±10	28±8	17+±6	15±6	15±8	21±10
HB cells	29±9	22±13	15±10	17±6	15±8	19±7
CHO cells	28 ±10	21±4	16±5	16±7	14±5	19±6

Table 3.1: Summary of all tether force measurements performed in the study. Values for the forces are given in pN.

3.3.4 The tether force is independent on the chemical nature of the cantilever surface

Experiments in which the chemical nature of the cantilever surface was changed were conducted to clarify that the tether force is independent of the nature of the attachment. AFM tips coated with poly-L-lysine or collagen were used to extract tethers from CHO cells and no significant differences were found in tether force (26 ± 7 pN and 29 ± 7 pN, respectively; compare with 28 ± 10 pN, for untreated cantilever; see Table 3.1). These results are consistent with earlier observations that tether growth, once underway, does not depend on the chemical nature of the attachment of tethers to the force transducer [37].

Histograms of tether forces measured between distinct plateaus for untreated CHO, HB, and endothelial cells are presented in Fig. 3.6 (upper row). In all histograms, a Gaussian fit was used to identify the average force needed to pull a single tether. At the pulling rate used (3 μm/s), the tether forces did not show significant variation among CHO cells (28 ± 10 pN), HB cells (29 ± 9 pN), and endothelial cells (29 ± 10 pN). These results suggest that small differences in membrane composition, surely present across the three strongly differing cell lines, do not significantly affect the magnitude of the tether force. Differences in

membrane composition could affect the initiation force. In addition, they provide further support for the ubiquitous character of tether formation resulting from local external forces acting on cells, and suggest that multiple tether formation may represent an important mechanism for cell attachment. The rather broad distribution of the forces (ΔF) observed in our histograms results from the heterogeneity in the properties of the membrane across the cell surface. This heterogeneity could be, in part, the consequence of the varying association of the cytoskeleton and the glycocalyx with the membrane.

3.3.5 Role of membrane-associated macromolecules

Treatment of cells with latrunculin A (LATA) is well known to disrupt the actin cytoskeleton in a concentration-dependent manner and leads to significant changes in overall morphology [18, 81]. In particular, transmembrane proteins (e.g., cadherins, integrins) lose their attachment to F-actin [19]. Thus, LATA treatment results in the concentration-dependent decoupling of the actin cytoskeleton from the plasma membrane. As expected, the tether force drops in an concentration dependent manner (Fig. 3.7). In our experiments, this effect is evident from the rounding of the cells and is manifest in the 50% reduced magnitude (for 1 μM LATA concentration) of the observed tether forces for all cell types (Fig. 3.6, middle row). More interestingly, a noticeable narrowing of the force distribution is observed in the histograms. The changes in width obtained from the standard deviation of Gaussian fits were found to be 4, 2, and 10 pN for endothelial, HB, and CHO cells, respectively. This narrowing could be a direct

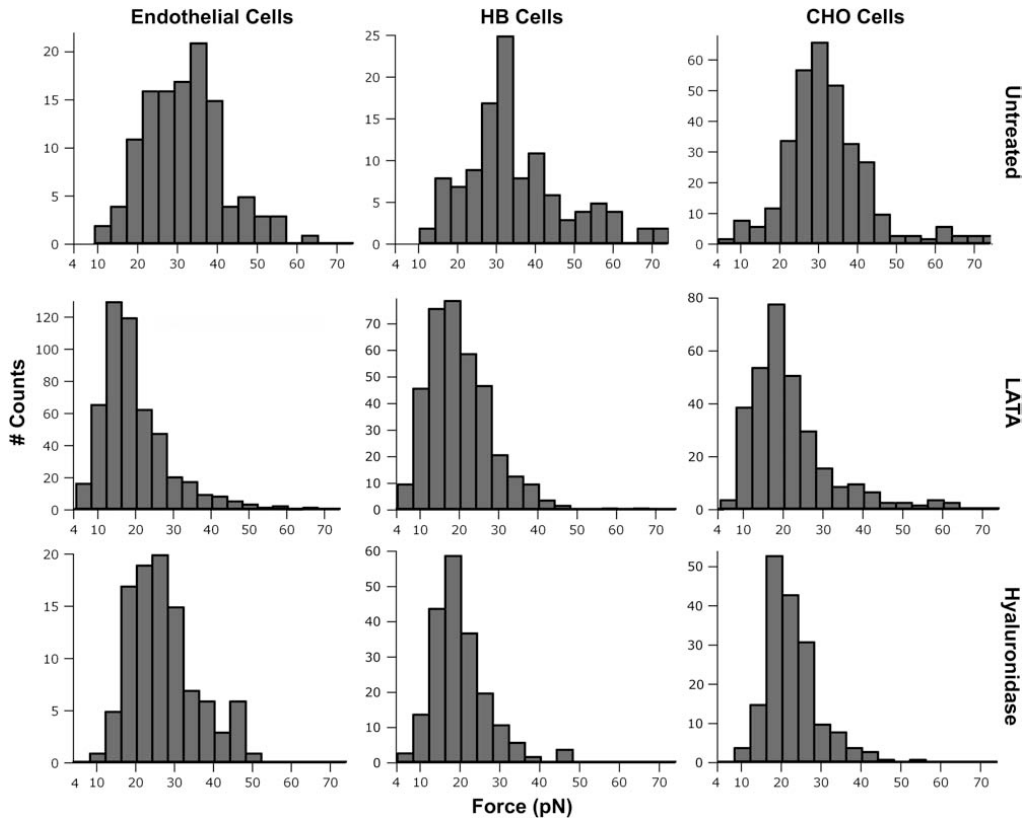

Figure 3.6: Single-tether force distributions for untreated and treated cells. Note the narrowing of these distribuations upon LATA or hyaluronidase treatment. Results shown are for 1 μM LATA and 500 IU/ml hyaluronidase concentrations [98].

consequence of the LATA-induced homogenization of membrane properties over the surface of the cell. LATA treatment reached its maximal effect at 0.2 μM (see Table 3.1) – a value in good agreement with the previously reported in vitro F-actin/LATA equilibrium dissociation constant, Kd = 0.2 μM.

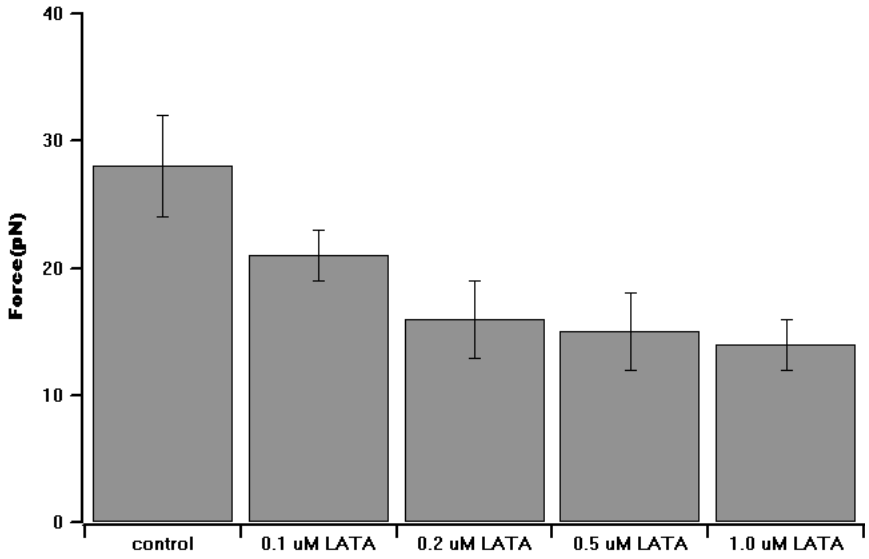

Figure 3.7: The tether force F decreases as the concentration of latrunculin A increases untill it reaches 0.2 μM.

The glycocalyx backbone hyaluronan of CHO, HB, and endothelial cells was disrupted by treatment with hyaluronidase. Hyaluronidase cleaves hyaluronan into disaccharides, which, in the present context, is equivalent to digesting part of the glycocalyx [107]. The tether force measured after hyaluronidase treatment was 30% lower than for untreated cells (Fig. 3.6, bottom row and Table 3.1). As with the experiments using LATA, one again observes a narrowing in the force distribution (at least for the HB and CHO cells, with the respective changes in width of 4 and 8 pN; for the endothelial cells, the width remained

unchanged), suggesting that the glycocalyx also contributes to the heterogeneity of plasma membrane properties. Overall, these findings show the importance of the macromolecular networks on both the intra- and extracellular sides of the cell membrane in the biomechanical integrity of the cell.

3.3.6 Discussion

Formation of a tether requires large changes in membrane curvature. The associated energy cost depends on the biomechanical properties (i.e., bending rigidity, effective surface tension [60, 65]) of the bilayer, as well as its association with the cytoskeleton and glycocalyx. AFM provides an alternative means to directly probe these properties through multiple tether extraction and pulling studies. Among the three cell lines used in our experiments, at the applied pulling rate, no major variation in single tether forces was found, implying that specific local cell membrane characteristics in these three cell types do not influence the growth of tethers. This finding also suggests that multiple tether formation is a ubiquitous phenomenon that can be initiated by nonspecific binding between a cell and its environment (e.g., other cells), and it is primarily a property of the plasma membrane itself that may be utilized in vastly differing circumstances.

Our measured values of tether forces are in good agreement with previously published data ranging from 10 to 60 pN for a variety of immobilized cells. Tether forces similar to those reported here have been measured at comparable pulling rates for fibroblasts [74], melanoma cell lines [24], neuronal growth cone membranes [23], and red blood cells [88]. In contrast to previous studies using optical

traps and micropipette aspiration that have the ability to extract individual tethers, with the AFM cantilever we simultaneously extracted multiple tethers, but retained the sensitivity to detect the loss of individual tethers as the membrane reservoir was gradually depleted. Initiation of multiple tether extraction requires overcoming a large initial potential barrier visible in the force profiles in Fig. 3.5. The force required to overcome the initial adhesion is typically larger than the maximum force that can be attained using optical traps or micropipette aspiration. One must therefore be careful how much surface area contacts the cell when using these techniques to ensure that the number of tethers extracted does not exceed the limiting forces. Attainment of the forces necessary to initiate extraction of multiple tethers is possible with the AFM.

The step-like structures result from the detachment of the membrane tethers from the cantilever

The observation of discrete force steps in our experiments raises the question of the origin of these rupture-like events. First, tethers could snap along their length. However, this would require overcoming close-to-lytic membrane tensions and, correspondingly, as experiments [25] and theory [30] indicate, forces of 100 pN, considerably higher than our measured values. Second, it has been suggested that heterogeneities within the membrane could locally decrease its tension and lead to tether fission [2]. This effect is expected to be cell-type-dependent and thus not likely to act in our experiments, in which no significant differences in tether force were observed. Third, theory suggests that multiple tethers extracted locally from the membrane reservoir in synthetic vesicles could

fuse, but that pinning forces may prevent fusion [26]. The glycocalyx and the cytoskeleton, absent in synthetic vesicles, provide ample possibilities for local pinning, thus fusion of tethers in living cells is highly regulated by these structures. Since in our experiments at least one of these macromolecular networks is always intact, the probability for fusion should be quite low. Experimental confirmation of tether fusion in synthetic vesicles has recently been provided [20]. These experiments showed that as fusion proceeds, a sudden change, similar to the discontinuities in Fig. 3.5, occurs in the components of the pulling force. The components parallel and perpendicular to the axis of the fused tethers respectively decrease and increase abruptly, while the overall force remains constant (for a given membrane tension). Interestingly, these results also strongly suggest that, in our experiments, tethers do not fuse. Fusion of tethers takes time. In the experiments of Cuvelier et al. [20], under static conditions (no pulling force exerted) the velocity of fusion was found to be 80 μm/s, and thus the time for two tethers to fuse along a 12-μm section to be 150 ms. Fusion in living cells, if it takes place, should be considerably slower due to heterogeneities in the membrane. However, as results in Fig. 3.5 show, force-steps occur much faster at comparable tether length. In fact, with the time-resolution of our device ($<$10 ms), we can estimate the time of a force-step to be an order-of-magnitude less than the time needed for fusion. Finally, tethers can detach from the cantilever. Considering that we do not reach the force necessary for tether rupture, and our force-steps occur on a timescale inconsistent with the fusion of tethers, we can assume that the force-steps result from detachment of the tethers from the cantilever.

Simultaneously extracted tethers share the membrane reservoir

As we pull groups of tethers with the AFM cantilever, they typically break off one by one. The extended membrane is then reincorporated into the membrane reservoir and the process continues until all of the tethers are released. The rigidity of the plasma membrane, conferred through the properties of its intrinsic components and peripherally associated macromolecules, defines the limits of the reservoir available to form tethers. This aspect is best illustrated by the measurement of the extent of the membrane reservoir as shown in Fig. 3.8. When measured within an individual force elongation profile, the size of the membrane reservoir probed was found to be approximately constant for each rupture event between consecutive plateaus. This result suggests that, when probed locally with an AFM tip, multiple simultaneously extracted membrane tethers are equally coupled to the membrane reservoir of the cell.

Previous studies demonstrated that tether properties depend on both actin microfilaments and microtubules, major components of the cytoskeleton [74]. Our results support these earlier findings. Indeed, we observed an 50% decrease in tether force after the inhibition of actin polymerization, indicating that cytoskeletal integrity is crucial in the regulation of the membrane's biomechanical characteristics. In contrast to the rather well-established function of the intracellular cortical cytoskeleton in the biomechanical role of the cell membrane, relatively little is known about the role of the proteoglycan complexes covering the extracellular surface of the phospholipid bilayer. Our finding of a 30% decrease in single tether force due to the disruption of the glycocalyx highlights

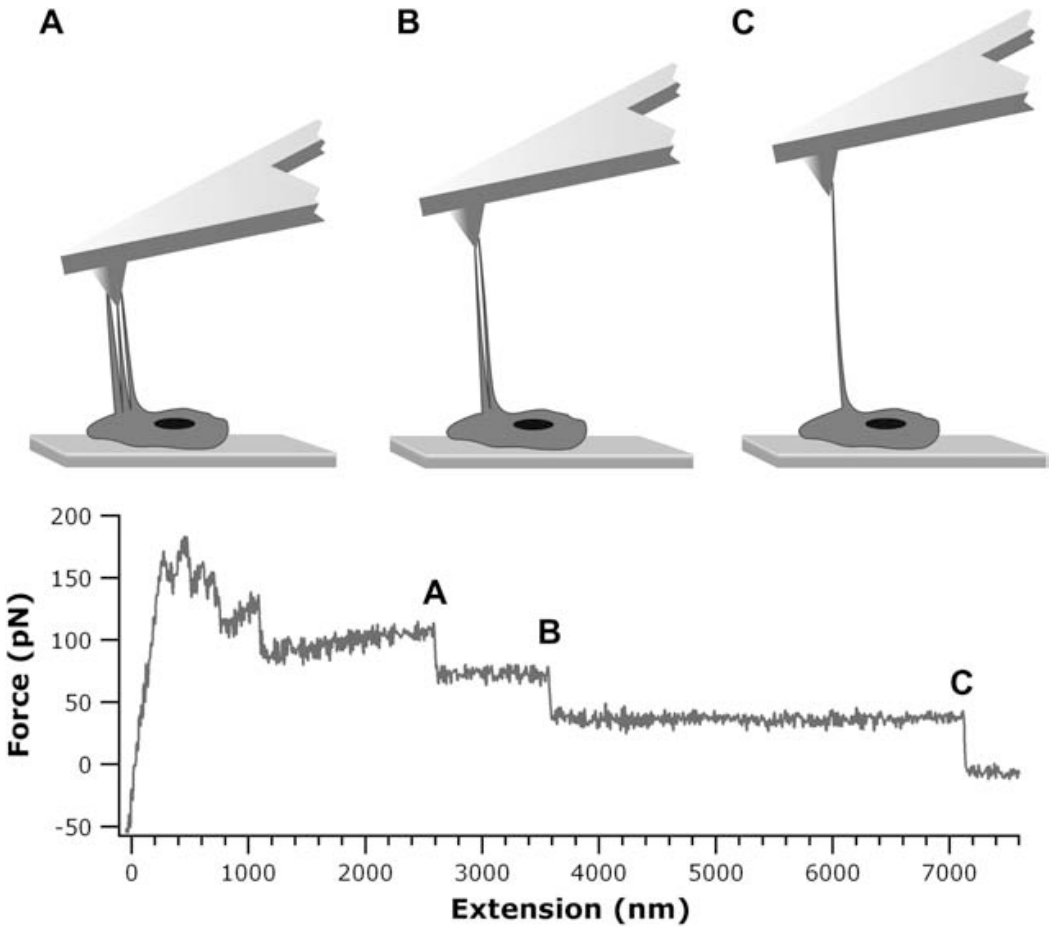

Figure 3.8: A force profile for an untreated endothelial cell is presented to illustrate the method of measuring the size of the membrane reservoir. The schematics on the top illustrate the state of the experiment at point A, B, and C along the retraction curve. A, B, and C correspond, respectively, to points with three tethers attached (L=3x2.6=7.8 μm, two tethers attached (L=2x3.6=7.2μm), and one tether attached (L=7.2μm). Here L stands for the total length of all simultaneously pulled tethers [98]

the importance of glycosaminoglycans on the mechanical properties of the lipid bilayer. Hence the hyaluronan backbone of the glycocalyx has a distinct effect on the mechanical properties of the plasma membrane in intact cells [107].

In summary, multiple tethers are manifest in AFM pulling experiments as plateaus separated by well-defined steps in the force profile. In this study, we evaluated the force required to pull individual tethers directly from the measurement of these force steps. Therefore, each force histogram presented in Fig. 3.6 represents an ensemble of measurements performed at many different positions on many cells. It is expected that, over the entire cell surface, heterogeneity exists in the coupling between the glycocalyx, cytoskeleton, and the membrane. Although the change in the peak values in the histograms after the two treatments is a specific measure of the coupling between the membrane and its peripheral macromolecular networks, the heterogeneity of the coupling is manifest through the broad distribution in the histograms for the nontreated cells. The marked narrowing of the histograms in LATA- and hyaluronidase-treated cells illustrates the reduction of this heterogeneity achieved through disruption of the cytoskeleton and glycocalyx.

Based on these findings, we propose that any cellular process that significantly affects the molecular networks interacting with the phospholipid bilayer influences its effective mechanical properties, and that this effect can be measured using atomic force microscopy. Furthermore, our results indicate that living cells can maintain multiple tethers. Local compositional modifications in the plasma membrane, as well as its association with the cytoskeleton and glycocalyx, through heterogeneities, can prevent the fusion of these coexisting

nanotubes and thus control their number. This may provide living cells with an additional mechanism to regulate their adhesive properties.

Chapter 4

Cholesterol effects on endothelial cell mechanical properties

In the previous chapter, we have developed a method to investigate cell mechanics by extracting multiple membrane tethers with the AFM. In this chapter, we apply this method to study the effect of cholesterol on endothelial cell (EC) mechanical properties. We will also discuss how change in EC mechanics are correlated with the development of atherosclerosis.

4.1 Background

Endothelial cell (EC) dysfunction is a strong predictor of cardiovascular disease (CVD) [38, 43, 86] since it develops in its early stages. A major risk factor for EC dysfunction is hypercholesterolemia, which is characterized by an increase in the levels of low- and very low- density lipoproteins (LDL and VLDL) and, in

particular, the oxidized form of LDL (oxLDL), as well as a decrease in the level of high-density lipoproteins (HDL). Hypercholesterolemia causes the formation and accumulation of plaque deposits in the arteries, which results in atherosclerosis. Recruitment of monocytes and leucocytes from the blood to the intima of the vessel wall is a primordial event in atherogenesis. This recruitment has been shown to relate with cell inflammation response. Under the hypercholesterolemic condition, the native LDL passes through the endothelium and accumulates in the arterial intima, where it undergoes oxidation and glycation. The oxidized LDL (and its components) can induce transcriptional activation of genes for several adhesion molecules (mainly VCAM-1 and ICAM-1) in the endothelial cells (called endothelial activation). Expression of the adhesion proteins will enhance the attachment of monocytes to the endothelium. Once strongly adherent to the endothelial cell, the monocytes transmigrate through the endothelial cell junctions (diapedesis) to the intima where they extensively internalize the modified LDL via scavenger receptors (CD36 and SR-A) and ultimately turn into foam cells. Foam cells secrete many kinds of pro-inflammatory cytokines, which amplify the local inflammatory response, further activate the endothelial cells, promote the transmigration of monocytes, and enhance transportation of LDL to the intima [67]. This progression continues as long as the hypercholesterolemetic condition remains (Fig. 4.1).

However, atherosclerotic lesions do not uniformly distribute in the blood vessel, they tend to form at brach points of arteries, which experience disturbed rather than laminar flow. This is due to the atheroprotective genes that are shear-stress sensitive. For example, nitric oxide arising from endothelial nitric

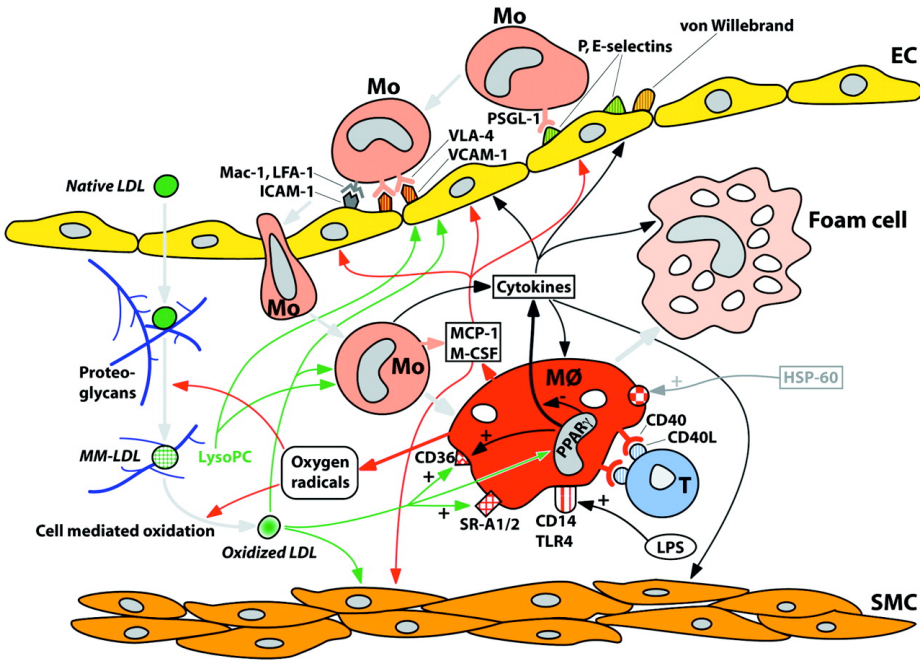

Figure 4.1: Foam cell formation in the intima. LDL passes through the endothelium to the intima, where it undergoes glycation and oxidation. The modified LDL induces cell inflammation response, which enhances the expression of certain adhesion molecules in the endothelial cells. As a consequence, more and more monocytes adhere to the endothelium and transmigrate to the intima, where they internalize the modified LDL and ultimately become foam cells. Figure form [67].

oxide synthase, a shear-stress sensitive gene, can inhibit VCAM gene expression, thus protect the vessel from lesion formation [16]. Thus, endothelial cells act as mechanical sensors that respond to external mechanical stimulati (shear stress) which in turn regulate cell behavior (gene expression). Extensive research has been done on shear-stress transduction and signalling by endothelial cells (for reviews, refer to [79]). However, less focus has been placed on the endothelial cell mechanical properties, especially the EC physical properties under hypocholesterolemic conditions.

Numerous experiments have demonstrated that cell mechanics plays an important role in regulating multiple cellular functions such as cell migration, proliferation, and cell differentiation [15,35,92]. As one specific example, it has been shown that under the same shear stress, increase of membrane fluidity by benzyl alcohol exhibited 3- to 5-fold enhancement of basal GTPase activity, while increase of membrane rigidity by adding cholesterol to the liposome decreased shear stress-induced activation of G proteins [40].

In this study, using the method developed in the previous chapter, I focus on endothelial cell mechanical properties under hypercholesterolemic conditions and correlate the change of cell mechanical properties with the development of atherosclerosis.

4.2 "Cell control by membrane-cytoskeleton interaction" [92]

Many cell functions are mechanically sensitive. For example, the rate of endocytosis is inversely related to the effective cell surface tension, because when the endocytic vesicles form, they need to overcome the load from the membrane. The higher the membrane tension is, the more difficult it is to form such vesicles and the lower is the endocytosis rate [22, 92]. Similar mechanism exists when cells form the lamellipodia at the leading edge [75, 92].

In animal cells, the origin of the membrane tension is mainly the adhesion of membrane to the cytoskeleton. Unlike the liposomes, which have no cytoskeleton, the membranes of animal cells strongly attach to the underlying cytoskeleton. When the cells need to protrude or form the endocytic vesicles, they need to break the linkages between the membrane and cytoskeleton. Thus membrane-cytoskeleton interaction becomes the core factor in affecting cell functions.

Cell membrane-cytoskeleton interaction can be quantified by membrane tether extraction. When membrane tethers form, the lipid bilayer needs to be separated from the underlying cytoskeleton and flow to the tethers. The force needed to extract tethers (tether force) is greatly affected by the membrane-cytoskeleton interaction. Under the same condition, if the cytoskeleton is dismantled, the tether force decreases. The difference of the tether force before and after cytoskeleton disruption reflects the strength of the interaction between the membrane and the cytoskeleton. We will use this rationale to investigate cholesterol effects on EC membrane-cytoskeleton interaction, and study the effects on cell functions.

4.3 Cholesterol effects on cell membrane-cytoskeleton interaction

The level of membrane cholesterol is an important factor in determining the physical properties of the lipid bilayer, such as its fluidity [9, 17, 105] and elastic modulus [31, 66]. Specifically, in case of artificial vesicles, the addition of cholesterol increases membrane stiffness [66]. In contrast to model membranes, Byfield et al. [12] showed that cholesterol depletion of bovine aortic endothelial cells significantly decreased cell deformability, as assessed by measuring the length of deformed membrane aspirated into a glass micropipette. Latrunculin-induced disassembly of the F-actin network abrogated the stiffening effect. However, micropipette aspiration does not allow determining whether the stiffening effect of cholesterol depletion is due to the reorganization of the cytoskeleton, the modifications in membrane-cytoskeleton interaction or both.

A study by Kwik and coworkers [54] showed that membrane cholesterol depletion decreased the lateral protein mobility in skin fibroblasts and this effect resulted from changes in the underlying actin network's architecture, again implicating the cytoskeleton. These observations clearly illustrate that cholesterol manipulation affects cells more globally than just through their membranes [54].

In the present study we used AFM-based force spectroscopy to quantitatively investigate the effect of cholesterol on membrane-cytoskeleton adhesion. In the AFM technique one measures the force needed to pull a tether at a constant velocity (i.e. tether force) and then analyzes the dependence of the tether force on the pulling velocity [8,29,42,44]. Using this method, we quantified membrane-

cytoskeleton interactions in bovine aortic endothelial cells and determined the effective surface viscosities of the cell membrane at different levels of cholesterol content. In addition, fluorescence recovery after photobleaching (FRAP) [4, 28, 78] was used to measure the lateral diffusion of a lipid analog $DiIC_{12}$ in the membrane.

Fig. 4.2 A represents an experimental tether extraction curve and Fig. 4.2 B shows the corresponding analysis of the tether force (explained in the previous chapter).

4.3.1 Results

Cholesterol depletion/enrichment significantly increases/decreases the threshold tether force

The mean tether force at each specific pulling speed was determined by the Gaussian fit to the resultant histogram (Fig. 4.2 B), which represents at least 15 cells and 500 step events (Fig. 4.2 A). Cell cholesterol level after cholesterol modulation was verified (Fig. 4.3 inset) as previously described [57]. The threshold tether force, and the effective surface viscosity of the membrane, were determined from the linear fit (Fig. 4.3 A) to the data. We found that cholesterol depletion greatly increased F_0 ($P< 0.01$), whereas cholesterol enrichment decreased it ($P<0.05$) (Fig.4.3 B and Table 4.1). Furthermore, cholesterol enrichment significantly ($P<0.01$) decreased the surface viscosity (Fig.4.3 A and Table 4.1), whereas cholesterol depletion did not change this quantity ($P>0.05$) (Fig.4.3 A and Table 4.1).

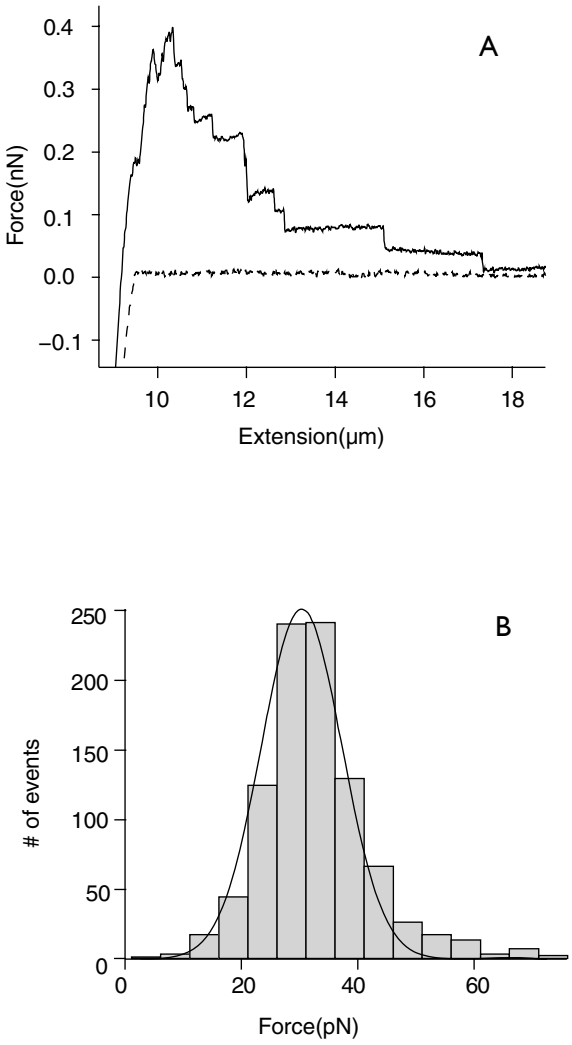

Figure 4.2: A: A typical force vs extension curve. The dotted line corresponds to the approach curve and the solid line is the retraction curve. On the retraction curve, several step-like structures are clearly discernible, which correspond to the sequential detachment of individual tethers from the cantilever. The shown retraction curve corresponds to an experiment performed with a control cell at 3 μm/s. B: Histogram constructed from the data (size of the steps) collected in the control experiments at 3 μm/s. The solid line is the Gaussian fit to the histogram, which gives the mean value of the tether force, 33 pN.

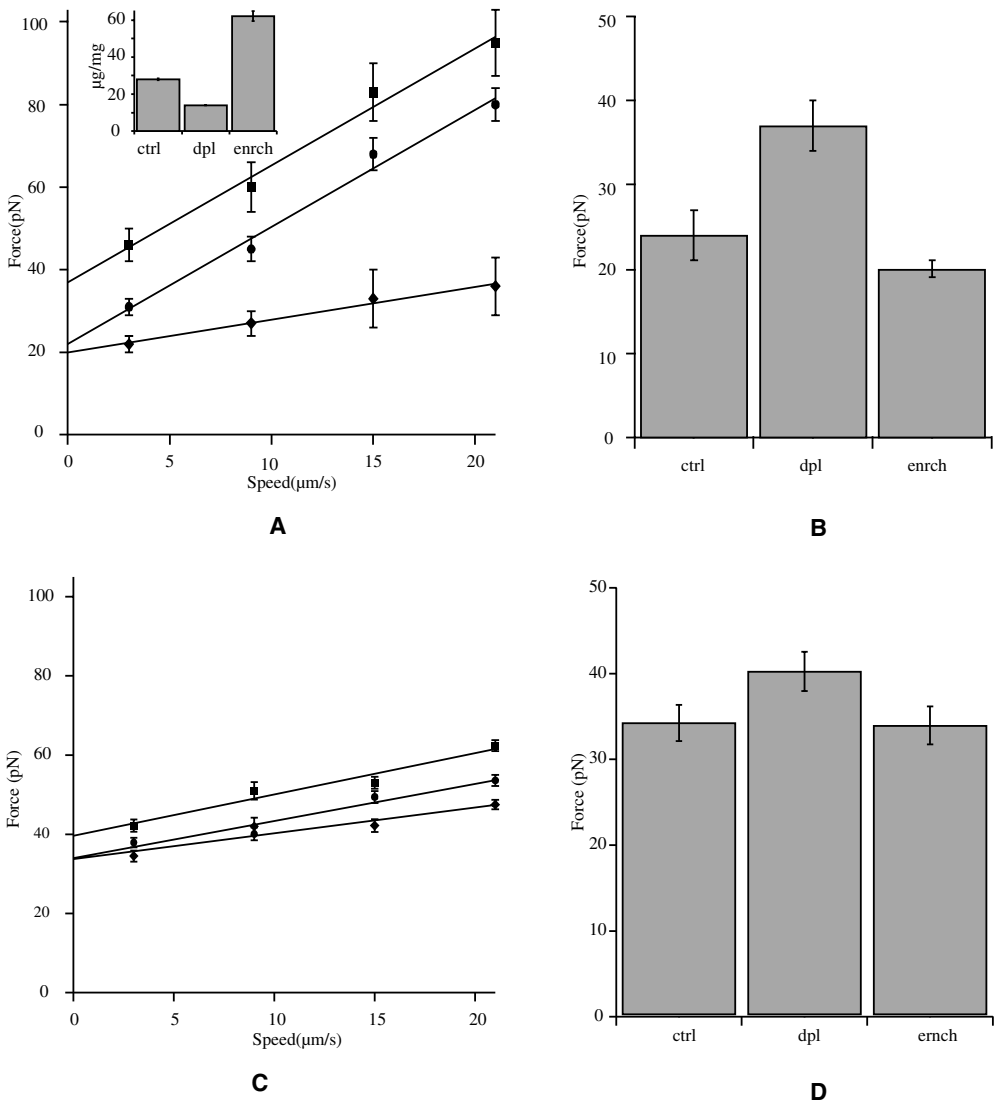

Figure 4.3: A and C: Tether force vs tether growth velocity at room temperature (A) and 37^{o}C (C). The solid lines are linear fits to the corresponding data sets (control, •; depletion ■; enrichment, ♦). Inset in A, cholesterol level measured by GLC. ctrl, control; dpl, cholesterol depleted; enrch, cholesterol enriched. The values of slopes ($\sim \eta_{eff}$) and intercepts (F_0) are listed in Table 4.1. B and D: Bar graphs for F_0 at room temperature (B) and 37^{o}C (D). Error bars in A and C represent S.E. obtained from the experimental data points. Errors in the bar graphs represent the error of the linear fit to the data. All six R^2 values were larger than 0.97.

	F_0(pN)			η(pN ·s/μm)		
	37^{o}C	22 ^{o}C	Lat A (22 ^{o}C)	37^{o}C	22 ^{o}C	Lat A (22 ^{o}C)
Control	34±2	24 ± 4	14±2	0.15 ±0.03	0.5±0.05	0.1±0.04
Cholesterol depleted	40 ±2	37 ±3	17 ±1	0.16±0.03	0.4±0.05	0.1±0.02
Cholesterol enriched	34±1	20 ±1	18±1	0.10±0.02	0.1±0.02	0.1±0.02

Table 4.1: Threshold pulling force (F_0) and the effective surface viscosity (η_{eff}).

Disruption of F-actin abrogates the effect of cholesterol on the tether force

The tether force strongly depends on the integrity of F-actin [23, 24, 98]. To test the F-actin component of the tether force, cells were exposed to 1 M latrunculin A, an F-actin depolymerizing agent [96]. As expected, fewer actin fibers were observed in latrunculin treated cells (Fig.4.4 B panels d-f). Although there was no latrunculin in the CO_2 independent medium (in which the experiments were carried out), we did not observe cell recovery in either morphology or tether force, indicating that the drug remained in the cells for the entire duration of the measurements (1-1.5 hours). Disruption of F-actin resulted in a significant decrease in the values of F_0 and η_{eff} for both the control and cholesterol depleted cells (Fig.4.4 A and Table 4.1). However, latrunculin did not significantly affect these quantities in cholesterol enriched cells. In addition, after latrunculin treatment we found no statistical difference in and among control, cholesterol depleted and enriched cells ($P > 0.05$; Fig.4.4 A and Table 4.1).

Cellular cholesterol content affects cell morphology

DIC microscopy was used to study the effect of differential cholesterol treatment on cell morphology. Blind experiments (see Employed Methods and Techniques) were performed to minimize bias in the interpretation of the images. Cholesterol depleted cells appeared smaller and thicker (Fig.4.5 A) than control cells (Fig.4.5 B), while cholesterol enriched cells could be resolved by their increased blebbing (Fig.4.5 C).

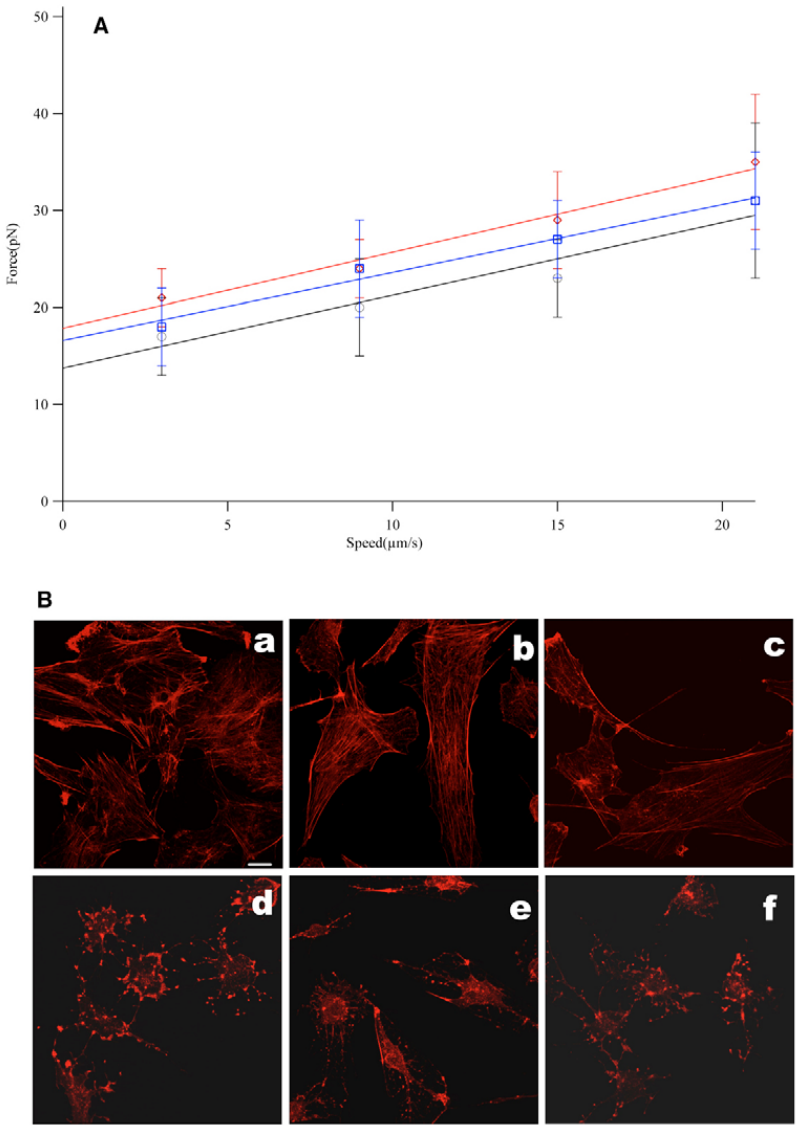

Figure 4.4: A: Tether force vs tether growth velocity after latrunculin A treatment (◯, control; □, cholesterol depleted; △, cholesterol enriched). Values of the intercepts and slopes are listed in Table 4.1. Error bars represent S.E. (note that the error bars overlap). B: Confocal images of the actin cytoskeleton for control (a, d), cholesterol-depleted (b, e), cholesterol enriched (c, f) BAECs, without (top row) or with (bottom row) latrunculin A treatment. Bar, 10 μm.

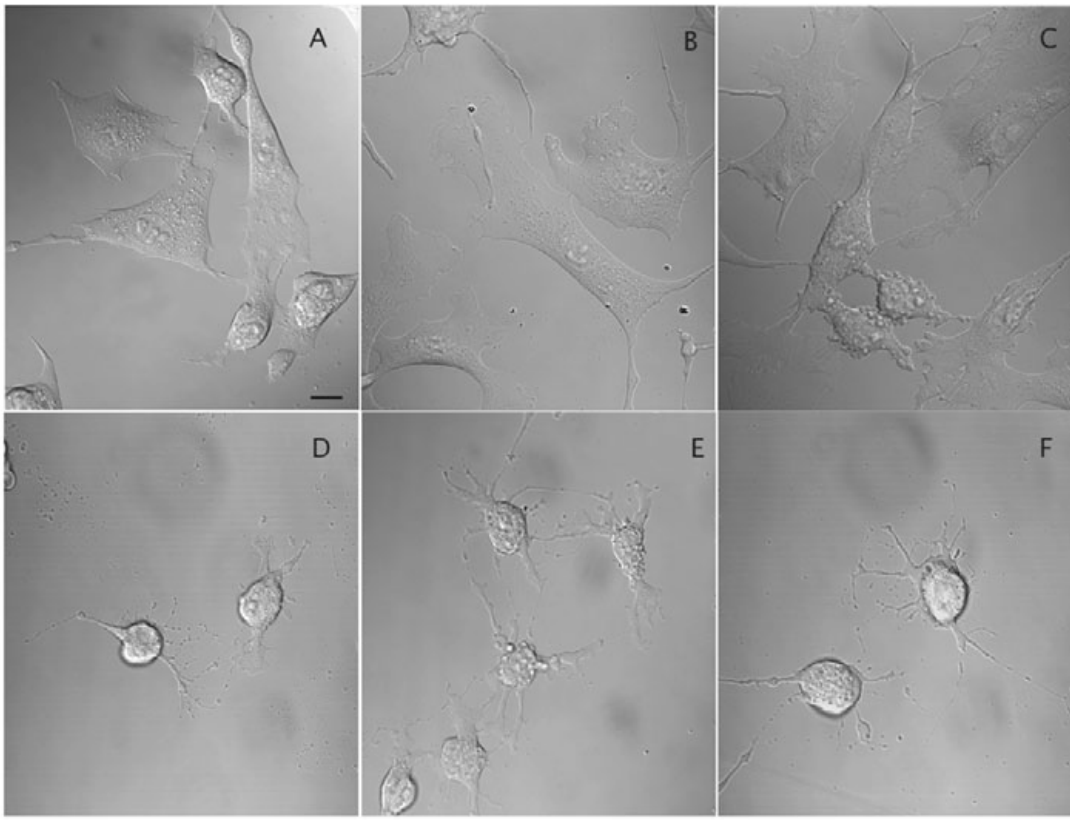

Figure 4.5: DIC images of cells with different cholesterol content. Cholesterol-depleted (A, D), control (B, E), cholesterol-enriched (C, F) BAECs, without (top row) or with (bottom row) latrunculin A treatment. Latrunculin A treated cells show a similar spherical morphology independently of cholesterol content. Bar, 10 μm.

Cellular cholesterol content affects variability in tethers

If the plasma membrane were not connected to the cytoskeleton (the case of artificial lipid vesicles), no differences between tethers would be expected. Thus, variability in tethers could also provide information on membrane-cytoskeleton association. Therefore, we performed a systematic study on the width of the histograms, constructed from the step-like events shown in Fig. 4.2, in all treatment cases. As results in Table 4.2 show, cholesterol depletion significantly increased variability, whereas cholesterol enrichment had a much smaller effect. Latrunculin A treatment renders cells considerably more homogeneous in all three cases (control, depletion and enrichment). These findings are consistent with the results presented earlier. Cholesterol depletion enhances membrane-cytoskeleton interaction and thus makes tethers less homogeneous. Upon latrunculin A treatment, this enhanced membrane-cytoskeleton interaction is abrogated and, as a consequence, tethers become more homogeneous.

	S_{total}
Control	7.1
Control+Lat A	6.4
Cholesterol depleted	22.9
Cholesterol depleted + Lat A	10.2
Cholesterol enriched	8.7
Cholesterol enriched + Lat A	7.5

Table 4.2: Tether variability.

Cholesterol depletion suppresses lateral diffusion in the membrane

Following cholesterol depletion or enrichment, cells were labeled with $DiIC_{12}$ for the FRAP measurements, as described in the Employed Methods and Techniques. Recovery curves after photobleaching (Fig. 4.6 A) were analyzed using the software described in [93]. Cholesterol depletion resulted in the decrease of $DiIC_{12}$ lateral mobility ($P<0.01$; Fig. 4.6 B), while cholesterol enrichment had no statistically significant effect (Fig. 4.6 B). We also studied how changes in the actin cytoskeleton affect the diffusion coefficient of $DiIC_{12}$. Cells were treated with 1 μM latrunculin A after cholesterol depletion or enrichment as described in the Employed Methods and Techniques. Disruption of F-actin had little to no effect on $DiIC_{12}$ mobility for either control and cholesterol enriched cells (Fig. 4.6 B). However, latrunculin treatment of cholesterol depleted cells resulted in significant increase in the diffusion coefficient (Fig. 4.6 B). Furthermore, similarly to the threshold tether force and effective surface viscosity (see above), after latrunculin treatment we found no statistical difference in the value of the diffusion constant among control, cholesterol depleted and enriched cells.

Cholesterol enrichment reduces bond force

Earlier work has confirmed that tether formation can reduce the force exerted on the specific bonds (the bond force, F_b) between endothelial cells of the vascular wall and leukocytes, and thus result in increased chance of adherence between the two cell types [37, 73, 87, 89]. To clarify how this finding may be affected by differential cholesterol conditions, we determined the time dependence of L

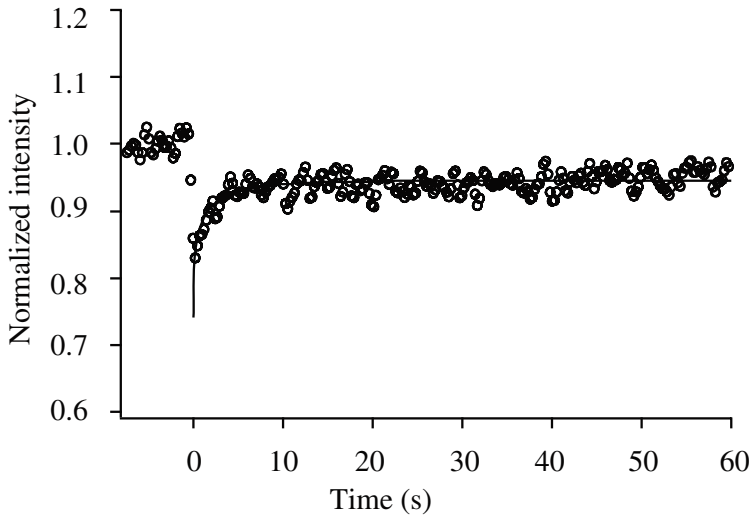

A

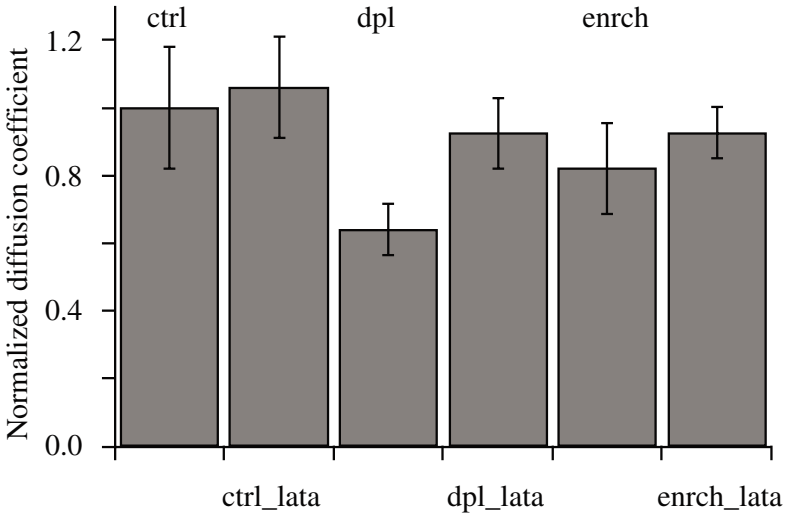

B

Figure 4.6: A: A typical recovery curve in a control FRAP experiment. The fluorescence intensity is normalized to the average fluorescence intensity before photobleaching. B: Diffusion coefficients in the various treatment cases (normalized to the value for the control). ctrl, control; dpl, cholesterol depleted; enrch, cholesterol enriched; lata, latrunculin A treated.

(tether length) and F_b for tethers connecting a leukocyte to an endothelial cell (see Employed Methods and Techniques). We found that after cholesterol enrichment, L and F_b respectively increase (Fig. 4.7 A) and decrease (Fig. 4.7 B) much faster than in the case of control and cholesterol-depleted cells. This result is consistent with the finding that cholesterol enrichment leads to decreased effective surface viscosity (Fig. 4.3 A,C). Interestingly, cholesterol depletion had no strong effect on either L or F_b. Increased tether length and reduced bond force both favor the slowing down of circulating leukocytes and, as a consequence, the possible accumulation of cells in the vicinity of the endothelium. Thus, increase in the endothelial cell membrane cholesterol level may be an initial step in atherosclerotic plaque formation.

4.3.2 Discussion

Formation of membrane tethers requires significant changes in membrane curvature. The associated energy cost depends on the biomechanical properties of the bilayer, as well as its association with the cytoskeleton [23, 92]. Studies on membrane tether extraction in general can help to understand the association between the membrane and the cytoskeleton, a factor particularly relevant to the processes of secretion and signaling [92]. By pulling membrane tethers using AFM, we found that cholesterol has significant effect on membrane-cytoskeleton adhesion. Specifically, we showed that cholesterol depletion enhances interaction between the membrane and the cytoskeleton and by this makes it harder to pull membrane tethers; cholesterol enrichment on the other hand weakens

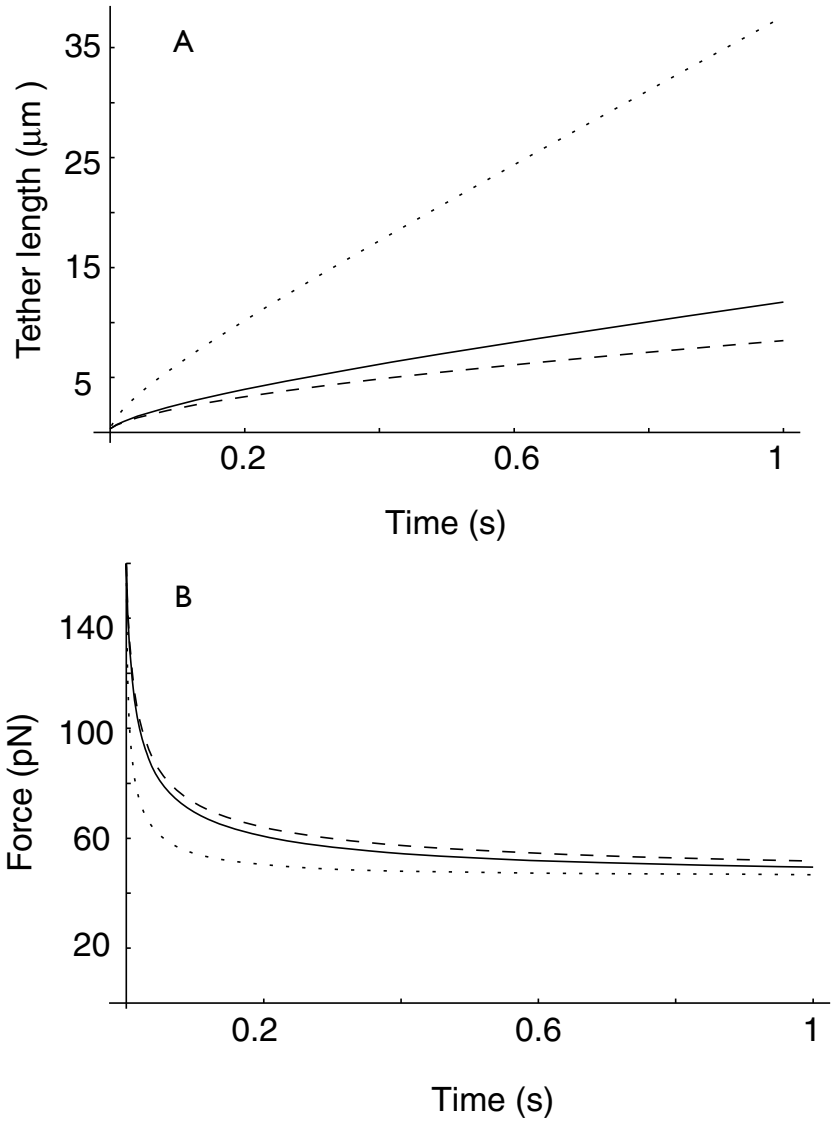

Figure 4.7: A: Tether length vs time, calculated using Eq. 2.1 on page 18 (see Employed Methods and Techniques). The tether grows much faster after cholesterol enrichment (dotted line) compared with the control (solid line) and cholesterol depleted (dashed line) cases. The curves for control and cholesterol depletion are similar. B: The estimated force acting on a bond between an endothelial tether and a leukocyte. After cholesterol enrichment (dotted curve), initially, the bond force decreases much faster than in the control (solid curve) and cholesterol depleted (dashed curve) cases. The curves for the control and cholesterol depletion are again similar.

the adhesion. Furthermore, our observations indicate that the increase in stiffness, following cholesterol depletion, originates primarily from the strengthened membrane-cytoskeleton adhesion and not from changes in the membrane itself. We also showed that, unexpectedly, cholesterol enrichment decreases the effective surface viscosity of the membrane as estimated from the tether force vs. tether growth velocity, whereas cholesterol depletion has no effect. Finally, we showed that cholesterol depletion but not cholesterol enrichment affects the lateral diffusion of the lipids in the membrane by FRAP. Taken together, these findings show that changes in the level of membrane cholesterol have profound effects on membrane-cytoskeleton interaction but specific mechanisms underlying the different effects are not fully understood yet. Our general conclusion is that change in membrane-cytoskeleton adhesion is a key factor in determining biomechanical properties of the cell envelope in aortic endothelial cells.

Earlier studies on lipid vesicles have shown that elevation of membrane cholesterol increases the stiffness of artificial lipid bilayers, as assessed by microaspiration analysis [66]. However, using the same experimental approach, Byfield et al. have shown that the stiffness of the cellular envelope of aortic endothelial cells is increased when cellular cholesterol level decreases while no change in stiffness was observed when the cells were enriched with cholesterol. They suggested, therefore, that cholesterol depletion may increase cellular stiffness by strengthening membrane-cytoskeleton interactions. Our current results strongly support this hypothesis by showing that after cholesterol depletion, considerably larger force is needed to pull membrane tethers. We also found that after F-actin disruption, the threshold tether force of the cholesterol depleted cells and control cells

became statistically indistinguishable. These results are consistent with those of Byfield et al. [12] showing that disruption of F-actin abrogates the stiffening effect induced by cholesterol depletion. These studies illustrate that cholesterol depletion affects the cell through the cytoskeleton network rather than locally along its membrane.

The contribution to the tether force by membrane-cytoskeleton adhesion, F_{ad}, can be estimated as follows:

$$F_{ad} = F_0 - F_0^{lata} \tag{4.1}$$

where F_0 and F_0^{lata} are the threshold tether force before and after latrunculin treatment, respectively. Since latrunculin treatment leads to the disruption of the F-actin network (Fig. 4.4 B, panel d-f), F_{ad} is directly related to the strength of the membrane-cytoskeleton interaction. The values of for control, depleted, and enriched cells are 10, 20, and 2 pN respectively (Fig. 4.8). The high value for the cholesterol depleted cell suggests strong interaction between the membrane and cytoskeleton, whereas the lower value for the cholesterol enriched cells indicates weak membrane-cytoskeleton interaction. Membrane-cytoskeleton interaction is essential for the membrane to conform to the cytoskeleton. Blebs will form when the membrane detaches from the cytoskeleton [91]. This suggests that the weakened membrane-cytoskeleton adhesion after cholesterol enrichment may result in the formation of blebs. Our studies using DIC imaging, as shown in Fig. 4.5 C, indeed show this to be the case.

It is important to note, however, that cholesterol enrichment did not have

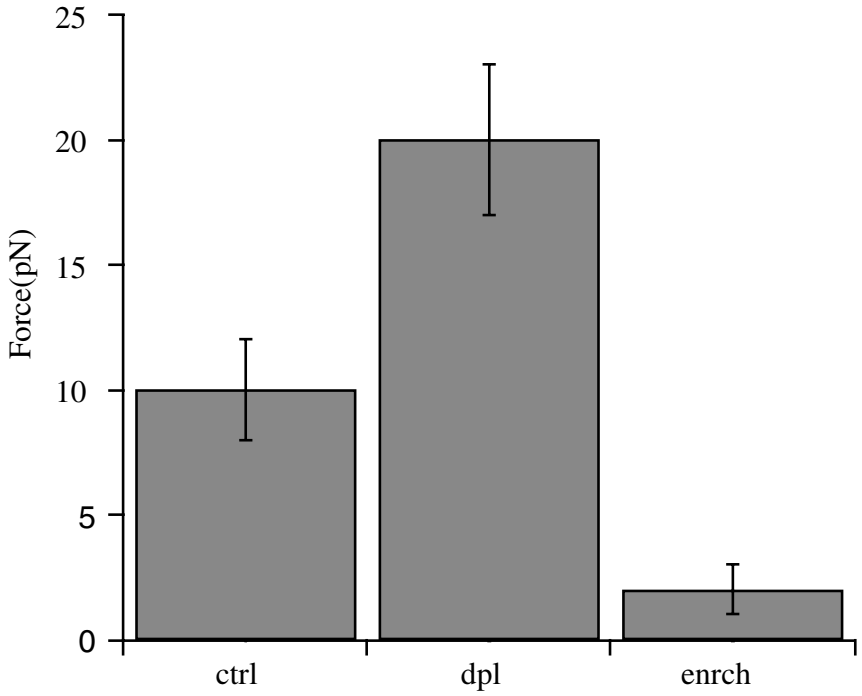

Figure 4.8: The estimated membrane-cytoskeleton adhesion force, F_{ad}, calculated using Eq. 4.1 on page 61. Values of F_{ad} for cholesterol depleted (dpl) and cholesterol enriched (enrch) cells are both significantly ($P < 0.05$) different from the control (ctrl).

any significant effect on endothelial stiffening estimated by microaspiration [12] in contrast with our findings. This discrepancy between results obtained with the two different methods suggests that microaspiration measurements involve both the membrane and the cytoskeleton (both being aspirated into the micropipette), whereas tether pulling with AFM mainly probes the adhesive contact between the membrane and the cytoskeleton.

Another important finding of this study is that cholesterol enrichment results in a significant decrease of the effective surface viscosity whereas cholesterol depletion has no effect. The effective membrane surface viscosity is determined by multiple factors, such as membrane properties, inter-bilayer slip, and the slip between the membrane and cytoskeleton [44]. Among these three contributions, the most significant is the slip between the membrane and cytoskeleton, as shown by Marcus [62], where latrunculin A treatment of neutrophils was found to decrease the effective surface viscosity from 1.1 pN·s/μm to close to zero. Our experiments support this finding: after 1 μM latrunculin A treatment, the effective surface viscosity decreases from 0.5 to about 0.1 pN·s/μm for the control and cholesterol depleted cells. This decrease in surface viscosity is most probably due to the loss of bonds linking the membrane to the cytoskeleton [62]. Therefore, a decrease in membrane viscosity in cholesterol-enriched cells is consistent with the decrease in membrane-cytoskeleton adhesion under these conditions. The fact that no further decrease in the effective membrane viscosity is observed upon latrunculin treatment in cholesterol enriched cells (Table 4.1, page 51), suggests that enrichment itself already significantly decreased the membrane-cytoskeleton interaction and therefore additional latrunculin treatment is largely ineffective.

Interestingly, in cholesterol-depleted cells the increase in F_0 is not accompanied with the increase in membrane viscosity. One possible explanation for this effect is that the increase in the slip between the cytoskeleton and the inner layer of the membrane that arises from an increase in membrane-cytoskeleton adhesion is compensated by the opposite effect on one of the other components that contribute to the membrane viscosity.

Another approach to address the role of membrane cholesterol in determining membrane fluidity is measuring the lateral diffusion of lipid molecules using FRAP, a conventional method to measure membrane lateral diffusion constants. Our study shows that after cholesterol depletion, the lateral diffusion of $DiIC_{12}$ decreased by about 30%, whereas cholesterol enrichment had no significant effect (Fig. 4.6 B). These observations are consistent with the earlier studies of Kwik et al. [54] and Kenworthy et al. [50] showing that cholesterol depletion increases the immobile fraction of HLA I proteins and decreases the diffusion coefficients of both raft and non-raft proteins. Vrljic et al. [102] also showed that the diffusion coefficients of $DiIC_{12}$, native and GPI-lined I-Ek decreased significantly when cholesterol was depleted from Chinese Hamster Ovary cells. Cholesterol enrichment was shown to have no effect on the lateral diffusion coefficients of either membrane proteins or membrane lipids [50, 102]. Also, consistent with the earlier studies, disrupting F-actin abrogated the difference in the diffusion coefficients between cholesterol depleted and control cells (Fig. 4.6 B). This implies that the suppression of lateral diffusion of $DiIC_{12}$ after cholesterol depletion is also related to the cytoskeleton.

An intriguing question is why the impact of cholesterol on η_{eff}, as measured

by AFM, is different from its impact on D, as measured by FRAP. On theoretical grounds, it is expected that an increase in D implies a decrease in η_{eff} [85]. However, in our study, cholesterol enrichment significantly reduced η_{eff}, but had no appreciable effect on D. Conversely, cholesterol depletion had no effect on η_{eff}, but significantly decreased D. One possible explanation is that AFM and FRAP measure distinct membrane properties. A more profound reason may be that our FRAP study tests only the outer leaflet of the plasma membrane (where the diffusion of $DiIC_{12}$ takes place), whereas AFM tests both (since tethers and thus η_{eff} are sensitive to the interconnection between the two leaflets). Therefore, the outcome of the FRAP experiments is affected less by membrane-cytoskeleton adhesion. Indeed, results in Fig. 4.6 B show a slight increase in D for control and enriched cells upon latrunculin A treatment. In cholesterol-depleted cells enhanced membrane-cytoskeleton adhesion may affect the movement of a lipid molecule even in the outer leaflet. Upon dismantling this adhesion, D becomes the same as in the other two cases. (The reason why depletion does not affect η_{eff} was discussed earlier.)

Changes in membrane-cytoskeleton adhesion are expected to have major impact on numerous cell functions, such as endocytosis, cell migration and membrane resealing (reviewed in [92]). We therefore expect, that an increase in membrane-cytoskeleton adhesion following cholesterol depletion makes it more difficult to form endocytic vesicles, slows down the rate of endocytosis, prevents the formation of membrane processes (such as lamellipodia protrusion), and affects cell morphology. Consistent with this expectation, Subtil et al. [97] showed that cholesterol depletion reduces the rate of internalization of transferrin recep-

tors by preventing the coated pits to detach from the plasma membrane. The authors proposed that cholesterol depletion changes the cells biomechanical properties. Conversely, cholesterol enrichment was shown to enhance endocytosis [90]. It is also important to note that while depleting cellular cholesterol with MβCD is not physiological, it was shown that exposing endothelial cells to oxLDL also results in cholesterol depletion from endothelial caveolae [7]. Furthermore, the effects of MβCD-induced cholesterol depletion on endothelial biomechanics were shown to be remarkably similar to the effects of exposing the cells to oxLDL [13].

Reduced membrane-cytoskeleton adhesion and decreased effective surface viscosity may have important implications in the development of atherosclerosis. Adhesion of circulating monocytes to the endothelium and thus reduction in their rolling are important components in the atherogenic process [21, 36, 80]. Experiments and numerical simulations demonstrate that formation of membrane tethers reduces the force exerted on specific bonds (i.e. selectin/PSGL-1) and increases bond lifetime, which results in increased chance of adherence of neutrophils to the endothelium [37, 73, 87, 89]. Our calculation clearly shows that after cholesterol enrichment the force exerted on the specific bond formed between an endothelial tether and a leukocyte decreases much faster than in the control or depleted cases (Fig. 4.7 B). As a consequence, bond lifetime will increase, which facilitates and stabilizes the rolling process. This implies that cholesterol enrichment may increase the probability of adherence of monocytes to endothelium, an observation consistent with experimental findings [69, 70]. In conclusion, based on AFM tether pulling and FRAP measurements, we showed that alterations in the level of membrane cholesterol lead to significant changes

in membrane-cytoskeleton adhesion, which in turn may affect important cellular and physiological processes.

4.4 The molecular mechanism of cholesterol induced cell stiffening

From the above study, it is clear that cholesterol modulation affects EC membrane-cytoskeleton interaction and consequently cell functions. However, the molecular mechanism for such change needs further study. Previous studies showed that the lipid molecule, PIP2, is the dominant linker between the membrane and the cytoskeleton (Fig. 4.9, a simple schematic of the interaction). Sequestration of PIP2 dramatically decreases membrane-cytoskeleton interaction, at least for fibroblasts [76, 77, 92]. There is also evidence showing that cholesterol modulation affects PIP2 concentration and/or distribution along the cell periphery [54]. Thus, we focused on PIP2 and investigated the relationship of PIP2 concentration/distribution, cholesterol modulation and membrane-cytoskeleton interaction.

4.4.1 Neomycin treatment mimics cholesterol depletion effects

Neomycin, an antibiotic was shown to be able to sequester PIP2 [3, 54]. The tether force was measured after exposing the cells to 0.01 M neomycin sulfate for 24 hours. Fig. 4.10 shows that after neomycin treatment, F_0 increases as also

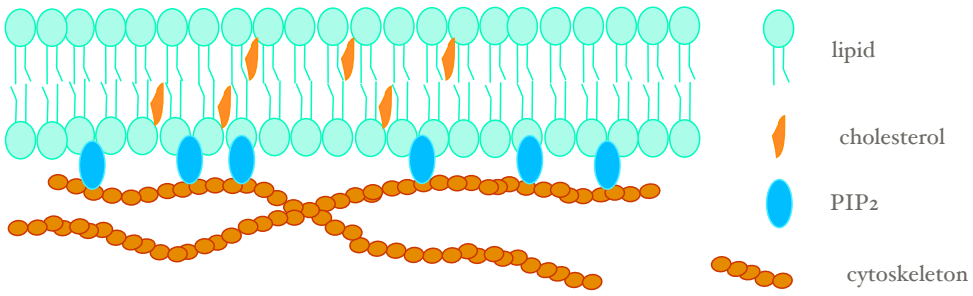

Figure 4.9: A schematic showing that PIP2 is the linker between the membrane and cytoskeleton. In reality, how PIP2 interacts with cytoskeleton (directly or indirectly) is not clear.

found in the case of cholesterol depletion. This result contradicts the assumption that PIP2 is the dominant linker because if that were the case one would expect F_0 to decrease.

However, one problem with the antibiotic is that the interaction is not very specific. To overcome this problem, another method was used to sequester PIP2.

4.4.2 Expression of Pleckstrin Homology (PH)-GFP

Cells were transfected with a plasmid expressing a GFP-tagged PH domain from phospholipase C-δ. After cells express the protein, the PH domain specifically binds PIP2 (Fig. 4.11).

In the experiments, we only extract tethers from the green cells, which successfully express the GFP-tagged PH domain (Fig. 4.12). Compared with neomycin treatment, this method is much more specific in sequestering PIP2. The preliminary data shows that the transfected cells have higher F_0, though not as high as the value for neomycin treated cells. In this aspect, it is consis-

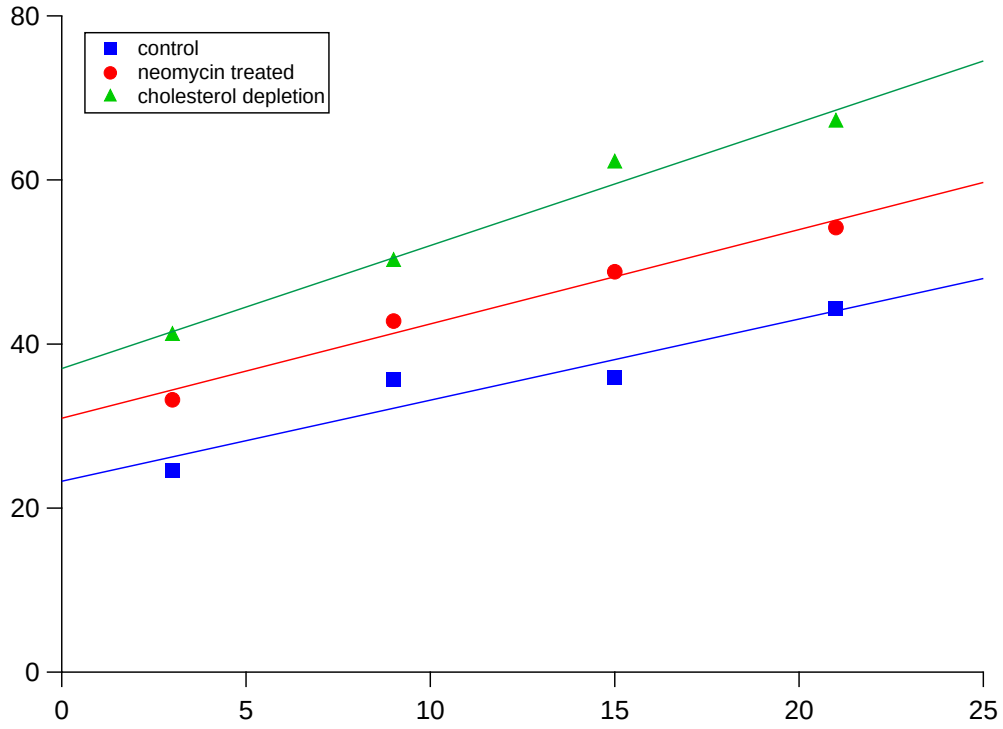

Figure 4.10: Sequestration of PIP2 using neomycin mimics cholesterol depletion effects on EC mechanics.

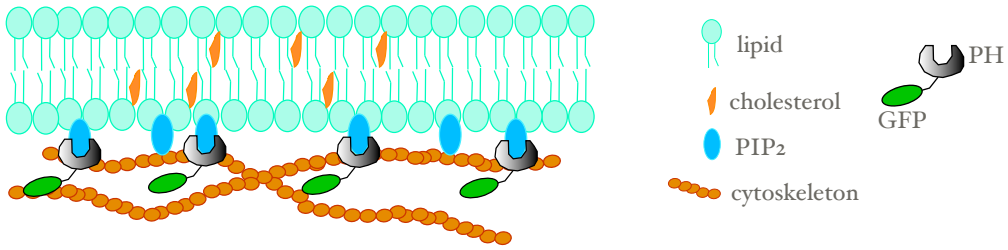

Figure 4.11: Sequestration of PIP2 with the gene transfection. After the cells express the protein, the PH-domain specifically binds the PIP2 so that PIP2 cannot link to the cytoskeleton.

tent with the neomycin treatment, meaning that PIP2 sequestration increases F_0. However, more control experiments are needed to arrive at this conclusion with confidence, especially because the transfection agents themselves seem to have significant effects on the tether force.

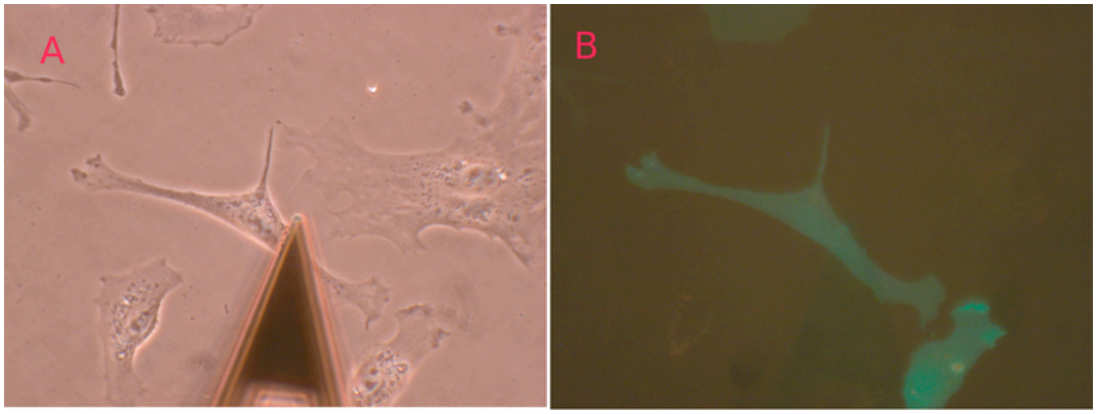

Figure 4.12: The experiments on the transfected cells. A: the phase contrast image of the cell with the cantilever atop. B: The same cells under the fluorescence microscope. In the tether measurement, only the green cells are considered.

In summary, our preliminary data shows that cholesterol depletion induced cell stiffening is correlated with PIP2 distribution or concentration in cells. However, the results seem to contradict the assumption that PIP2 is the dominant linker between the membrane and cytoskeleton. A different mechanism may be involved. However, at this point, further investigation are needed.

Chapter 5

Theories of membrane tether formation

There are different theories to explain membrane tether formation. Based on the functional relationship of the tether force (F) and the tether pulling speed (v_t), they can be divided into two classes: the linear theory and the non-linear theory.

5.1 The linear theory

In 1996, Hochmuth and coworkers [44] developed a theory to describe membrane tether formation. This theory has been widely and successfully used to describe tether formation in many cell types though it was originally developed to describe tether formation in neuronal growth cones. In this theory, the tether force is a

linear function of the tether pulling speed

$$F = F_0 + 2\pi\eta_{eff}v_t \tag{5.1}$$

where F_0 is the minimum force to extract a tether and η_{eff} is the effective surface viscosity.

F_0 is determined by the membrane bending rigidity (B) and the effective membrane tension (T_{eff}). Unlike lipid vesicles which have a well defined membrane tension, for a real cell the effective membrane tension is defined as:

$$T_{eff} = T + \gamma \tag{5.2}$$

where T is the membrane tension as in the lipid vesicles, and γ is the energy of adhesion between the membrane and cytoskeleton. F_0 is related to B and T_{eff} by:

$$F_0 = 2\pi\sqrt{2BT_{eff}} \tag{5.3}$$

In animal cells with strong membrane-cytoskeleton interaction, F_0 is mainly determined by the membrane-cytoskeleton adhesion (γ) which is consistent with the experimental observations that after cytoskeleton disruption, F_0 decreases significantly.

The effective membrane surface viscosity (η_{eff}) is affected by three factors: the friction between the inner leaflet of the bilayer with the cytoskeletion, the interaction between the two leaflets, and the viscosity of the membrane itself. Normally, the disruption of the cytoskeleton also makes the effective surface

viscosity smaller.

5.2 The non-linear theory

In 2005, Heinrich and coworkers [42] provided a phenomenological non-linear model to describe tether formation in human neutrophils. In this model, the tether force has a weak power-law dependence on the tether pulling speed,

$$F = 60 v_t^{0.25} \tag{5.4}$$

The origin of this power law relationship is the shear-thinning in the nonlinear Maxwell-like fluid. The authors claimed that such nonlinear relationship applies to pulling speeds from 0.4 μm/s to 150 μm/s. When the speed was lower than 0.4 μm/s, in their experimental condition, there were very few tethers detected [42].

One shortcoming of this theory is that it cannot describe the tether's behavior at very low speed, thus in the vicinity of minimal force required to extract tethers (i.e. F_0 in the linear theory, as given by Eq. 5.1). Later, by assuming that the tether radius changes during the pulling process, Brochard-Wyart et al derived another nonlinear relationship of $F(v)$:

$$F^3 - F F_0^2 = \alpha v_t \tag{5.5}$$

where α is a constant related to the membrane rigidity and membrane surface viscosity. This theory does provide the minimum force to extract membrane tethers (F_0).

5.3 Testing the theories

To test the different theories, a systematic study was done using BAECs with tether pulling speeds ranging from 1 μm/s to 40 μm/s. Due to technical difficulties, the experiments with speeds higher than 40 μm/s are not reliable. Fig. 5.1 shows the experiment results together with the theoretical fits. The linear fit using Eq. 5.1 gives better results than the nonlinear fit for our data. This is why in our speed regime, we used the linear model for the interpretation of the collected data, as presented in the previous chapters.

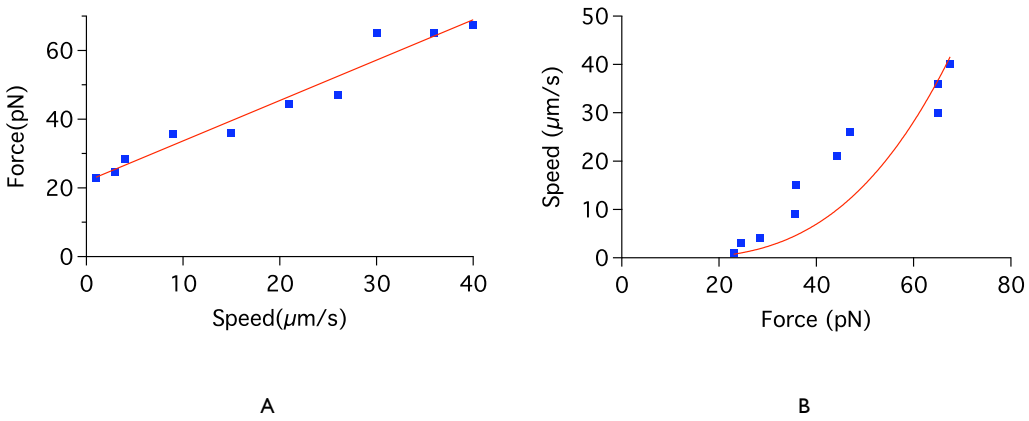

Figure 5.1: A: The linear fit using formula 5.1. B: The nonlinear fit using Eq. 5.5. Notice that the axes of B is different from that of A.

Chapter 6

Summary

We have developed a method to investigate cell mechanics using AFM by extracting membrane tethers. Using this method, we have systematically studied tether formation in a variety of cell types and concluded that tether formation is a ubiquitous phenomenon. We found that multiple tether can readily form in the investigated cells and these may play important role in the arrest of motile cells. The force needed to extract a tether is affected by both the cytoskeleton and the glacocalyx, the two macromolecular networks that sandwithc the cell membrane.

As a special application of the method, we used it to study cholesterol effects on EC mechanics. There is evidence showing that cholesterol affects the ability of cells to change shape, a factor that plays an important role in the development of atherosclerosis. By extracting membrane tethers from cells with different cholesterol content (control, cholesterol depleted or cholesterol enriched), we were able to evaluate the effect of cholesterol on EC mechanics, especially

on the membrane-cytoskeleton interaction, which is believed to control vital cell functions.

Our results show that cholesterol depletion of BAECs results in significant increase of membrane-cytoskeleton adhesion. As a consequence, cell motility and rate of endocytosis both decrease. On the other hand, cholesterol enrichment decreases the effective membrane surface viscosity, making the cells more liquid like. Based on a hydrodynamic model, we showed that the decreased membrane surface viscosity reduces the force exerted on the specific bonds between monocytes and endothelial cells, and consequently increases bond lifetime. This is consistent with the experimental observations that cholesterol enrichment favors the recruitment of the monocytes to the endothelium.

To investigate the molecular bases of these findings, we focused on the regulatory phospholipid, phosphatidylinositol 4,5-biophosphate (PIP2). Sequestration of PIP2 either by neomycin or by PH-PLC transfection mimics cholesterol depletion effects. This indicates that the effects of cholesterol modulation on EC mechanics may be through a complicated signal transduction process.

Bibliography

[1] S. Alexander, L. Hellemans, O. Marti, J. Schneir, V. Elings, P.K. Hansma, L. Matt, and G. John. An atomic-resolution atomic-force microscope implemented using an optical lever. *Journal of Applied Physics*, 65(1):164–167, 1989.

[2] J. M. Allain, C. Storm, A. Roux, M. B. Amar, and J. F. Joanny. Fission of a multiphase membrane tube. *Physical Review Letters*, 93(15):158104, October 2004.

[3] A. Arbuzova, K. Martushova, G. Hangyas-Mihalyne, A. J. Morris, S. Ozaki, G. D. Prestwich, and S. McLaughlin. Fluorescently labeled neomycin as a probe of phosphatidylinositol-4,5-bisphosphate in membranes. *Biochimica Et Biophysica Acta-Biomembranes*, 1464(1):35–48, March 2000.

[4] D. Axelrod, P. Ravdin, D.E. Koppel, J. Schlessinger, W.W. Webb, E.L. Elson, and T.R. Podleski. Lateral motion of fluorescently labeled acetylcholine receptors in membranes of developing muscle fibers. *Proc Natl Acad Sci U S A*, 73(12):4594–4598, 1976.

[5] M. Benoit, D. Gabriel, G. Gerisch, and H.E. Gaub. Discrete interactions in cell adhesion measured by single-molecule force spectroscopy. *Nat Cell Biol*, 2(6):313–317, 2000.

[6] G. Binnig, C.F. Quate, and C. Gerber. Atomic force microscope. *Physical Review Letters*, 56(9):930–933, 1986.

[7] A. Blair, P.W. Shaul, I.S. Yuhanna, P.A. Conrad, and E.J. Smart. Oxidized low density lipoprotein displaces endothelial nitric-oxide synthase (enos) from plasmalemmal caveolae and impairs enos activation. *J Biol Chem*, 274(45):32512–32519, 1999.

[8] F. Brochard-Wyart, N. Borghi, D. Cuvelier, and P. Nassoy. Hydrodynamic narrowing of tubes extruded from cells. *Proc Natl Acad Sci U S A*, 103(20):7660–7663, 2006.

[9] P. Brulet and H.M. McConnell. Lateral hapten mobility and immunochemistry of model membranes. *Proc Natl Acad Sci U S A*, 73(9):2977–2981, 1976.

[10] H. J. Butt and M. Jaschke. Calculation of thermal noise in atomic force microscopy. *Nanotechnology*, 6(1):1–7, 1995.

[11] H.J. Butt, M. Kappl, H. Mueller, R. Raiteri, W. Meyer, and J. Ruhe. Steric forces measured with the atomic force microscope at various temperatures. *Langmuir*, 15(7):2559–2565, 1999.

[12] F.J. Byfield, H. Aranda-Espinoza, V.G. Romanenko, G.H. Rothblat, and I. Levitan. Cholesterol depletion increases membrane stiffness of aortic endothelial cells. *Biophys J*, 87(5):3336–3343, 2004.

[13] F.J. Byfield, S. Tikku, G.H. Rothblat, K.J. Gooch, and I. Levitan. Oxldl increases endothelial stiffness, force generation, and network formation. *J Lipid Res*, 47(4):715–723, 2006.

[14] S. Chen and T.A. Springer. An automatic braking system that stabilizes leukocyte rolling by an increase in selectin bond number with shear. *J Cell Biol*, 144(1):185–200, 1999.

[15] A.M. Collinsworth, S. Zhang, W.E. Kraus, and G.A. Truskey. Apparent elastic modulus and hysteresis of skeletal muscle cells throughout differentiation. *Am J Physiol Cell Physiol*, 283(4):C1219–1227, 2002.

[16] P.R. Colville-Nash, S.S. Qureshi, D. Willis, and D.A. Willoughby. Inhibition of inducible nitric oxide synthase by peroxisome proliferator-activated receptor agonists: correlation with induction of heme oxygenase 1. *J Immunol*, 161(2):978–984, 1998.

[17] R.A. Cooper. Influence of increased membrane cholesterol on membrane fluidity and cell function in human red blood cells. *J. Supramol. Struct.*, 8(4):413–430, 1978.

[18] M. Coue, S.L. Brenner, I. Spector, and E.D. Korn. Inhibition of actin polymerization by latrunculin a. *FEBS Lett*, 213(2):316–318, 1987.

[19] D.R. Critchley. Focal adhesions - the cytoskeletal connection. *Curr Opin Cell Biol*, 12(1):133–139, 2000.

[20] D. Cuvelier, I. Derenyi, P. Bassereau, and P. Nassoy. Coalescence of membrane tethers: experiments, theory, and applications. *Biophysical Journal*, 88(4):2714–2726, April 2005.

[21] M. I. Cybulsky and M. A. Gimbrone. Endothelial expression of a mononuclear leukocyte adhesion molecule during atherogenesis. *Science*, 251(4995):788–791, February 1991.

[22] J. Dai, H.P.T. Beall, and M.P. Sheetz. The secretion-coupled endocytosis correlates with membrane tension changes in rbl 2h3 cells. *J Gen Physiol*, 110(1):1–10, 1997.

[23] J. Dai and M.P. Sheetz. Mechanical properties of neuronal growth cone membranes studied by tether formation with laser optical tweezers. *Biophys. J.*, 68(3):988–996, 1995.

[24] J. Dai and M.P. Sheetz. Membrane tether formation from blebbing cells. *Biophys. J.*, 77(6):3363–3370, 1999.

[25] J. Dai, M.P. Sheetz, X. Wan, and C.E. Morris. Membrane tension in swelling and shrinking molluscan neurons. *J Neurosci*, 18(17):6681–6692, 1998.

[26] I. Derenyi, F. Julicher, and J. Prost. Formation and interaction of membrane tubes. *Phys Rev Lett*, 88(23):238101, 2002.

[27] C.J. Edgell, C.C. McDonald, and J.B. Graham. Permanent cell line expressing human factor viii-related antigen established by hybridization. *Proc Natl Acad Sci U S A*, 80(12):3734–3737, 1983.

[28] M. Edidin, Y. Zagyansky, and T.J. Lardner. Measurement of membrane protein lateral diffusion in single cells. *Science*, 191(4226):466–468, 1976.

[29] E. Evans, V. Heinrich, A. Leung, and K. Kinoshita. Nano- to microscale dynamics of p-selectin detachment from leukocyte interfaces. i. membrane separation from the cytoskeleton. *Biophysical Journal*, 88(3):2288–2298, March 2005.

[30] E. Evans and F. Ludwig. Dynamic strengths of molecular anchoring and material cohesion in fluid biomembranes. *Journal Of Physics-Condensed Matter*, 12(8A):A315–A320, February 2000.

[31] E. Evans and D. Needham. Physical properties of surfactant bilayer membranes:thermal transition, elasticity, rigidity, cohesion and colloidal interactions. *J. Phys. Chem.*, 91:4219–4228, 1987.

[32] E.A. Evans and R.M. Hochmuth. Membrane viscoelasticity. *Biophys J*, 16(1):1–11, 1976.

[33] E.A. Evans and R.M. Hochmuth. Membrane viscoplastic flow. *Biophys J*, 16(1):13–26, 1976.

[34] M. Gerhard and M.A. Nabil. Novel optical approach to atomic force microscopy. *Applied Physics Letters*, 53(12):1045–1047, 1988.

[35] P.K. Ghosh, A. Vasanji, G. Murugesan, S.J. Eppell, L.M. Graham, and P.L. Fox. Membrane microviscosity regulates endothelial cell motility. *Nat Cell Biol*, 4(11):894–900, 2002.

[36] Jr. Gimbrone, M.A., M.I. Cybulsky, N. Kume, T. Collins, and N. Resnick. Vascular endothelium. an integrator of pathophysiological stimuli in atherogenesis. *Annals of the New York Academy of Sciences*, 748:122–131; discussion 131–132, 1995.

[37] G. Girdhar and J. Y. Shao. Membrane tether extraction from human umbilical vein endothelial cells and its implication in leukocyte rolling. *Biophysical Journal*, 87(5):3561–3568, November 2004.

[38] M.A. Gonzalez and A.P. Selwyn. Endothelial function, inflammation, and prognosis in cardiovascular disease. *Am J Med*, 115 Suppl 8A:99S–106S, 2003.

[39] J. Graham. *Mechanical Properties of Complex Biological Systems using AFM-Based Force Spectroscopy.* PhD thesis, University of Missouri-Columbia, 2005.

[40] S. Gudi, J.P. Nolan, and J.A. Frangos. Modulation of gtpase activity of g proteins by fluid shear stress and phospholipid composition. *Proc Natl Acad Sci U S A*, 95(5):2515–2519, 1998.

[41] B. Hegedus, A. Czirok, I. Fazekas, T. B'Abel, E. Madar'asz, and T. Vicsek. Locomotion and proliferation of glioblastoma cells in vitro: statistical

evaluation of videomicroscopic observations. *J Neurosurg*, 92(3):428–434, 2000.

[42] V. Heinrich, A. Leung, and E. Evans. Nano-to-microscale mechanical switches and fuses mediate adhesive contacts between leukocytes and the endothelium. *J Chem Inf Model*, 45(6):1482–1490, 2005.

[43] T. Heitzer, T. Schlinzig, K. Krohn, T. Meinertz, and T. Munzel. Endothelial dysfunction, oxidative stress, and risk of cardiovascular events in patients with coronary artery disease. *Circulation*, 104(22):2673–2678, 2001.

[44] R. M. Hochmuth, J. Y. Shao, J. W. Dai, and M. P. Sheetz. Deformation and flow of membrane into tethers extracted from neuronal growth cones. *Biophysical Journal*, 70(1):358–369, January 1996.

[45] R.M. Hochmuth, N. Mohandas, and Jr. Blackshear, P.L. Measurement of the elastic modulus for red cell membrane using a fluid mechanical technique. *Biophys J*, 13(8):747–762, 1973.

[46] B. G. Hosu, M. Sun, F. Marga, M. Grandbois, and G. Forgacs. Eukaryotic membrane tethers revisited using magnetic tweezers. *Physical Biology*, 4(2):67–78, June 2007.

[47] J. L. Hutter and J. Bechhoefer. Calibration of atomic-force microscope tips. *Review Of Scientific Instruments*, 64(7):1868–1873, July 1993.

[48] W.C. Hwang and R.E. Waugh. Energy of dissociation of lipid bilayer from the membrane skeleton of red blood cells. *Biophys J*, 72(6):2669–2678, 1997.

[49] A. Iglic, H. Hagerstrand, M. Bobrowska-Hagerstrand, V. Arrigler, and V. Kraij-Iglic. Possible role of phospholipid nanotubes in directed transport of membrane vesicles. *Physics Letters A*, 310(5-6):493–497, 2003.

[50] Anne K Kenworthy, Benjamin J Nichols, Catha L Remmert, Glenn M Hendrix, Mukesh Kumar, Joshua Zimmerberg, and Jennifer Lippincott-Schwartz. Dynamics of putative raft-associated proteins at the cell surface. *J Cell Biol*, 165(5):735–746, Jun 2004.

[51] G. Koster, M. VanDuijn, B. Hofs, and M. Dogterom. Membrane tube formation from giant vesicles by dynamic association of motor proteins. *Proc Natl Acad Sci U S A*, 100(26):15583–15588, 2003.

[52] A. Kultti, K. Rilla, R. Tiihonen, A. P. Spicer, R. H. Tammi, and M. I. Tammi. Hyaluronan synthesis induces microvillus-like cell surface protrusions. *Journal Of Biological Chemistry*, 281(23):15821–15828, June 2006.

[53] S. Kumar and J.H. Hoh. Probing the machinery of intracellular trafficking with the atomic force microscope. *Traffic*, 2(11):746–756, 2001.

[54] J. Kwik, S. Boyle, D. Fooksman, L. Margolis, M.P. Sheetz, and M. Edidin. Membrane cholesterol, lateral mobility, and the phosphatidylinositol 4,5-bisphosphate-dependent organization of cell actin. *Proc Natl Acad Sci U S A*, 100(24):13964–13969, 2003.

[55] C. A. Lamontagne and M. Grandbois. Pkc-induced stiffening of hyaluronan/cd44 linkage; local force measurements on glioma cells. *Experimental Cell Research*, 314(2):227–236, January 2008.

[56] C. Leduc, O. Campas, K.B. Zeldovich, A. Roux, P. Jolimaitre, L. Bourel-Bonnet, B. Goud, J.F. Joanny, P. Bassereau, and J. Prost. Cooperative extraction of membrane nanotubes by molecular motors. *Proc Natl Acad Sci U S A*, 101(49):17096–17101, 2004.

[57] I. Levitan, A.E. Christian, T.N. Tulenko, and G.H. Rothblat. Membrane cholesterol content modulates activation of volume-regulated anion current in bovine endothelial cells. *J Gen Physiol*, 115(4):405–416, 2000.

[58] S. Li, P. Butler, Y.X. Wang, Y.L. Hu, D.C. Han, S. Usami, J.L. Guan, and S. Chien. The role of the dynamics of focal adhesion kinase in the mechanotaxis of endothelial cells. *Proceedings of the National Academy of Sciences of the United States of America*, 99(6):3546–3551, 2002.

[59] Z. Li, B. Anvari, M. Takashima, P. Brecht, J.H. Torres, and W.E. Brownell. Membrane tether formation from outer hair cells with optical tweezers. *Biophys J*, 82(3):1386–1395, 2002.

[60] R. Lipowsky. The morphology of lipid membranes. *Curr Opin Struct Biol*, 5(4):531–540, 1995.

[61] O.H. Lowry, N.J. Rosebrough, A.L. Farr, and R.J. Randall. Protein measurement with the folin phenol reagent. *J Biol Chem*, 193(1):265–275, 1951.

[62] W.D. Marcus and R.M. Hochmuth. Experimental studies of membrane tethers formed from human neutrophils. *Ann Biomed Eng*, 30(10):1273–1280, 2002.

[63] A.B. Mathur, A.M. Collinsworth, W.M. Reichert, W.E. Kraus, and G.A. Truskey. Endothelial, cardiac muscle and skeletal muscle exhibit different viscous and elastic properties as determined by atomic force microscopy. *J Biomech*, 34(12):1545–1553, 2001.

[64] O. J. McCarty, S. A. Mousa, P. F. Bray, and K. Konstantopoulos. Immobilized platelets support human colon carcinoma cell tethering, rolling, and firm adhesion under dynamic flow conditions. *Blood*, 96(5):1789–1797, Sep 2000.

[65] D. Needham and R.M. Hochmuth. A sensitive measure of surface stress in the resting neutrophil. *Biophys J*, 61(6):1664–1670, 1992.

[66] D. Needham and R.S. Nunn. Elastic-deformation and failure of lipid bilayer-membranes containing cholesterol. *Biophysical Journal*, 58(4):997–1009, 1990.

[67] B. Osterud and E. Bjorklid. Role of monocytes in atherogenesis. *Physiol Rev*, 83(4):1069–1112, 2003.

[68] Eric Y H Park, McRae J Smith, Emily S Stropp, Karen R Snapp, Jeffrey A DiVietro, William F Walker, David W Schmidtke, Scott L Diamond, and Michael B Lawrence. Comparison of psgl-1 microbead and neutrophil

rolling: microvillus elongation stabilizes p-selectin bond clusters. *Biophys J*, 82(4):1835–1847, Apr 2002.

[69] Jr. Pritchard, K.A., S.M. Schwarz, M.S. Medow, and M.B. Stemerman. Effect of low-density lipoprotein on endothelial cell membrane fluidity and mononuclear cell attachment. *Am J Physiol*, 260(1 Pt 1):C43–49, 1991.

[70] Jr. Pritchard, K.A., R.R. Tota, J.H. Lin, K.J. Danishefsky, B.A. Kurilla, J.A. Holland, and M.B. Stemerman. Native low density lipoprotein. endothelial cell recruitment of mononuclear cells. *Arterioscler Thromb*, 11(5):1175–1181, 1991.

[71] R. Proksch, T. E. Schaffer, J. P. Cleveland, R. C. Callahan, and M. B. Viani. Finite optical spot size and position corrections in thermal spring constant calibration. *Nanotechnology*, 15(9):1344–1350, September 2004.

[72] M. Radmacher. Measuring the elastic properties of biological samples with the afm. *IEEE Eng Med Biol Mag*, 16(2):47–57, 1997.

[73] V. Ramachandran, M. Williams, T. Yago, D. W. Schmidtke, and R. P. McEver. Dynamic alterations of membrane tethers stabilize leukocyte rolling on p-selectin. *Proceedings Of The National Academy Of Sciences Of The United States Of America*, 101(37):13519–13524, September 2004.

[74] D. Raucher and M.P. Sheetz. Characteristics of a membrane reservoir buffering membrane tension. *Biophys J*, 77(4):1992–2002, 1999.

[75] D. Raucher and M.P. Sheetz. Cell spreading and lamellipodial extension rate is regulated by membrane tension. *J. Cell. Biol.*, 148(1):127–136, 2000.

[76] D. Raucher and M.P. Sheetz. Phospholipase c activation by anesthetics decreases membrane-cytoskeleton adhesion. *J Cell Sci*, 114(Pt 20):3759–3766, 2001.

[77] D. Raucher, T. Stauffer, W. Chen, K. Shen, S. L. Guo, J. D. York, M. P. Sheetz, and T. Meyer. Phosphatidylinositol 4,5-bisphoshate functions as a second messenger that regulates cytoskeleton-plasma membrane adhesion. *Cell*, 100(2):221–228, January 2000.

[78] E.A. Reits and J.J. Neefjes. From fixed to frap: measuring protein mobility and activity in living cells. *Nat Cell Biol*, 3(6):E145–E147, 2001.

[79] N. Resnick, H. Yahav, S. Schubert, E. Wolfovitz, and A. Shay. Signalling pathways in vascular endothelium activated by shear stress: relevance to atherosclerosis. *Curr Opin Lipidol*, 11(2):167–177, 2000.

[80] M.E. Rosenfeld, T. Tsukada, A.M. Gown, and R. Ross. Fatty streak initiation in watanabe heritable hyperlipemic and comparably hypercholesterolemic fat-fed rabbits. *Arteriosclerosis*, 7(1):9–23, 1987.

[81] C. Rotsch and M. Radmacher. Drug-induced changes of cytoskeletal structure and mechanics in fibroblasts: an atomic force microscopy study. *Biophys J*, 78(1):520–535, 2000.

[82] Giovanni; Cartaud Jean; Prost Jacques; Goud Bruno & Bassereau Patricia Roux, A.C. A minimal system allowing tubulation with molecular motors pulling on giant liposomes. *Proc Natl Acad Sci U S A*, 99(8):5394–5399, 2002.

[83] Amin Rustom, Rainer Saffrich, Ivanka Markovic, Paul Walther, and Hans-Hermann Gerdes. Nanotubular highways for intercellular organelle transport. *Science*, 303(5660):1007–1010, Feb 2004.

[84] J. E. Sader, I. Larson, P. Mulvaney, and L. R. White. Method for the calibration of atomic-force microscope cantilevers. *Review Of Scientific Instruments*, 66(7):3789–3798, July 1995.

[85] P.G. Saffman and M. Delbruck. Brownian motion in biological membranes. *Proc. Natl. Acad. Sci. USA*, 72(8):3111–3113, 1975.

[86] V. Schachinger and A.M. Zeiher. Atherosclerosis-associated endothelial dysfunction. *Z Kardiol*, 89 Suppl 9:IX/70–74, 2000.

[87] D.W. Schmidtke and S.L. Diamond. Direct observation of membrane tethers formed during neutrophil attachment to platelets or p-selectin under physiological flow. *J Cell Biol*, 149(3):719–730, 2000.

[88] J.Y. Shao and R.M. Hochmuth. Micropipette suction for measuring piconewton forces of adhesion and tether formation from neutrophil membranes. *Biophys J*, 71(5):2892–2901, 1996.

[89] J.Y. Shao, H.P. Ting-Beall, and R.M. Hochmuth. Static and dynamic lengths of neutrophil microvilli. *Proc Natl Acad Sci U S A*, 95(12):6797–6802, 1998.

[90] D.K. Sharma, J.C. Brown, A. Choudhury, T.E. Peterson, E. Holicky, D.L. Marks, R. Simari, R.G. Parton, and R.E. Pagano. Selective stimulation of caveolar endocytosis by glycosphingolipids and cholesterol. *Mol Biol Cell*, 15(7):3114–3122, 2004.

[91] M. P. Sheetz, J. E. Sable, and H. G. Dobereiner. Continuous membrane-cytoskeleton adhesion requires continuous accommodation to lipid and cytoskeleton dynamics. *Annual Review Of Biophysics And Biomolecular Structure*, 35:417–434, 2006.

[92] M.P. Sheetz. Cell control by membrane-cytoskeleton adhesion. *Nat Rev Mol Cell Biol*, 2(5):392–396, 2001.

[93] E. D. Siggia, J. Lippincott-Schwartz, and S. Bekiranov. Diffusion in inhomogeneous media: theory and simulations applied to whole cell photobleach recovery. *Biophys J*, 79(4):1761–1770, Oct 2000.

[94] A. Simon, T. Cohen-Bouhacina, M.C. Porte, J.P. Aime, J. Amedee, R. Bareille, and C. Baquey. Characterization of dynamic cellular adhesion of osteoblasts using atomic force microscopy. *Cytometry A*, 54(1):36–47, 2003.

[95] Stefanie Sowinski, Clare Jolly, Otto Berninghausen, Marco A Purbhoo, Anne Chauveau, Karsten Khler, Stephane Oddos, Philipp Eissmann,

Frances M Brodsky, Colin Hopkins, Bjrn Onfelt, Quentin Sattentau, and Daniel M Davis. Membrane nanotubes physically connect t cells over long distances presenting a novel route for hiv-1 transmission. *Nat Cell Biol*, 10(2):211–219, Feb 2008.

[96] I. Spector, N.R. Shochet, D. Blasberger, and Y. Kashman. Latrunculins–novel marine macrolides that disrupt microfilament organization and affect cell growth: I. comparison with cytochalasin d. *Cell Motil. Cytoskeleton*, 13(3):127–144, 1989.

[97] A. Subtil, I. Gaidarov, K. Kobylarz, M.A. Lampson, J.H. Keen, and T.E. McGraw. Acute cholesterol depletion inhibits clathrin-coated pit budding. *Proc Natl Acad Sci U S A*, 96(12):6775–6780, 1999.

[98] M. Sun, J.S. Graham, B. Hegedus, F. Marga, Y. Zhang, G. Forgacs, and M. Grandbois. Multiple membrane tethers probed by atomic force microscopy. *Biophys J*, 89(6):4320–4329, 2005.

[99] A. Torii, M. Sasaki, K. Hane, and S. Okuma. A method for determining the spring constant of cantilevers for atomic force microscopy. *Measurement Science & Technology*, 7(2):179–184, February 1996.

[100] Andreea Trache and Gerald A Meininger. Atomic force-multi-optical imaging integrated microscope for monitoring molecular dynamics in live cells. *J Biomed Opt*, 10(6):064023, 2005.

[101] A. Upadhyaya and M. P. Sheetz. Tension in tubulovesicular networks of golgi and endoplasmic reticulum membranes. *Biophysical Journal*, 86(5):2923–2928, May 2004.

[102] M. Vrljic, S.Y. Nishimura, W.E. Moerner, and H.M. McConnell. Cholesterol depletion suppresses the translational diffusion of class ii major histocompatibility complex proteins in the plasma membrane. *Biophys. J.*, 88(1):334–347, 2005.

[103] R.E. Waugh, A. Mantalaris, R.G. Bauserman, W.C. Hwang, and J.H. Wu. Membrane instability in late-stage erythropoiesis. *Blood*, 97(6):1869–1875, 2001.

[104] G. Xu and J. Y. Shao. Double tether extraction from human neutrophils and its comparison with cd4(+) t-lymphocytes. *Biophysical Journal*, 88(1):661–669, January 2005.

[105] X. Xu and E. London. The effect of sterol structure on membrane lipid domains reveals how cholesterol can induce lipid domain formation. *Biochemistry*, 39(5):843–849, 2000.

[106] E.G. Yarmola, T. Somasundaram, T.A. Boring, I. Spector, and M.R. Bubb. Actin-latrunculin a structure and function. differential modulation of actin-binding protein function by latrunculin a. *J Biol Chem*, 275(36):28120–28127, 2000.

[107] R. Zaidel-Bar, M. Cohen, L. Addadi, and B. Geiger. Hierarchical assembly of cell-matrix adhesion complexes. *Biochem Soc Trans*, 32(Pt3):416–420, Jun 2004.

[108] J.H. Zar. *Biostatistical Analysis*. Prentice Hall, Upper Saddle River, NJ., 1999.

[109] X. H. Zhang, E. P. Wojcikiewicz, and V. T. Moy. Dynamic adhesion of t lymphocytes to endothelial cells revealed by atomic force microscopy. *Experimental Biology And Medicine*, 231(8):1306–1312, September 2006.

VITA

Mingzhai Sun was born on February 2nd, 1979, in Juancheng, China. He finished his Bachelor degree in Chemical Physics and Master degree in Material Physics from the University of Science and Technology of China, in 2002. In the summer of 2002, he joined the Department of Physics and Astronomy at the University of Missouri-Columbia. He received his Ph.D in May 2008. He will continue his biological physics research as a Postdoctoral Fellow at Princeton University, NJ, USA.